

1 **Characterisation of mafic enclaves in the erupted products of Soufrière Hills Volcano,**  
2 **Montserrat 2009-2010**

3  
4 Melissa Plail<sup>1\*</sup>, Jenni Barclay<sup>1</sup>, Madeleine C. S. Humphreys<sup>2</sup>, Marie Edmonds<sup>3</sup>, Richard A.  
5 Herd<sup>1</sup> & Thomas Christopher<sup>4</sup>

6 <sup>1</sup> School of Environmental Sciences, University of East Anglia, Norwich, NR4 7TJ, UK

7 <sup>2</sup> Department of Earth Sciences, University of Oxford, South Parks Road, Oxford, OX1 3AN,  
8 UK

9 <sup>3</sup> Department of Earth Sciences, University of Cambridge, Downing Street, Cambridge, CB2  
10 3EQ, UK

11 <sup>4</sup> Montserrat Volcano Observatory, Flemings, Montserrat, West Indies

12 \*Corresponding author: m.plail@uea.ac.uk

13  
14 **Abstract**

15 Lavas from the current eruption of the Soufrière Hills Volcano, Montserrat exhibit evidence  
16 for magma mingling, related to the intrusion of mafic magma at depth. We present detailed  
17 field, petrological, textural and geochemical descriptions of mafic enclaves in andesite  
18 erupted during 2009-2010, and subdivide the enclaves into three distinct types. Type A are  
19 mafic, glassy with chilled margins and few inherited phenocrysts. Type B are more evolved  
20 with high inherited phenocryst contents and little glass, and are interpreted as significantly  
21 hybridised. Type C are composite, with a mafic interior (type A) and a hybrid exterior (type  
22 B). All enclaves define tight linear compositional trends, interpreted as mixing between a  
23 mafic end-member (type A) and host andesite. Enclave glasses are rhyolitic, owing to  
24 extensive crystallisation during quenching. Type A quench crystallisation is driven by rapid  
25 thermal equilibration during injection into the andesite. Conversely, type B enclaves form in  
26 a hybridised melt layer, which ponded near the base of the chamber and cooled more slowly.  
27 Vesiculation near the mafic-silicic interface resulted in disruption of the hybridised layer and  
28 the formation of the Type B enclaves. The composite enclaves represent an interface between  
29 types A and B, suggesting multiple episodes of mafic injection.

30 **Number of words: 8964**

31 **Number of tables: 6**

32 **Number of figures: 12**

33 **Number of references: 61**

34 **Abbreviated title: Mafic enclaves at SHV**

35

36 The process of magma mingling, where two or more magmas mix incompletely  
37 during magma storage in the crust, is commonly associated with arc volcanism (*e.g.* Pallister  
38 *et al.* 1992; Clynne 1999) and results in the formation of banded pumice and magmatic  
39 mafic enclaves (*e.g.* Bacon 1986; Clynne 1999; Browne *et al.* 2006b; Martin *et al.* 2006b).  
40 More complete mixing of magmas is inhibited by large contrasts in viscosity and density,  
41 reflecting differences in temperature, composition and crystallinity, and the relative  
42 proportions of the incoming and host magmas (Eichelberger 1980; Bacon 1986; Sparks &  
43 Marshall 1986). The textures of enclaves form in response to the local crystallisation  
44 conditions, and can yield information about the mingling processes or the dynamics of the  
45 intruding magma. For example, the presence of a diktytaxitic framework composed of  
46 elongate quench crystals and chilled enclave margins indicates rapid undercooling (Bacon  
47 1986). Enclaves without chilled margins and more tabular framework crystals can indicate  
48 that they were predominantly crystallised prior to incorporation into the host magma (solid-  
49 liquid mingling) (*e.g.* Eichelberger 1980; Coombs *et al.* 2002). Therefore these enclaves may  
50 represent the remnants of a fragmented vesiculated mafic layer from the silicic-mafic  
51 interface (Eichelberger 1980; Thomas & Tait 1997; Martin *et al.* 2006a). Formation of a  
52 discrete layer of mafic magma is typically thought to be a product of slow and small volume  
53 material injection, where viscosity, density and temperature contrasts between the two  
54 magmas are strong (Sparks & Marshall 1986). In contrast, enclaves that predominantly  
55 crystallised after incorporation into the host reflect direct injection of intruding magma into  
56 the host and therefore a more dynamic mingling relationship (Bacon 1986; Sparks &  
57 Marshall 1986; Clynne 1999). For example, at Unzen, Japan, Browne *et al.* (2006a) use  
58 textural differences to infer whether enclaves sampled represent the slower cooling of the  
59 centre of an intrusion or the silicic-mafic interface where there is a high degree of  
60 undercooling.

61 As well as mafic enclaves, disequilibrium textures within both the host rock and  
62 enclaves can also be used to track mingling dynamics. Examples of these disequilibrium

63 textures are sieve-textured plagioclase, reverse zoning in orthopyroxene, breakdown of  
64 amphibole and clinopyroxene-rimmed quartz (*e.g.* Singer *et al.* 1995; Tepley *et al.* 1999;  
65 Nakagawa *et al.* 2002; Browne *et al.* 2006b). Disequilibrium may be caused by variable  
66 heating of the host magma from input of hotter magma (*e.g.* Tepley *et al.* 1999), or  
67 incorporation of the host phenocrysts into the incoming magma (*e.g.* Ruprecht & Wörner  
68 2007), which may then be recycled back into the host magma via disaggregation (*e.g.* Clyne  
69 1989, 1999; Browne *et al.* 2006b; Humphreys *et al.* 2009). Combined textural, petrological  
70 and geochemical analysis of magmatic enclaves and coexisting phenocrysts can therefore  
71 provide insights into the nature of the mixing magmas, the dynamics of the mingling process,  
72 and changes that may be occurring during mixing.

73 Soufrière Hills represents a unique opportunity to study the process of magma  
74 mingling in an active system. Magma intrusion at depth appears to have been quasi-  
75 continuous throughout the eruption, based on excess sulphur emissions (Edmonds *et al.* 2001,  
76 2010) and inflation during eruptive pauses (Mattioli & Herd, 2003; Elsworth *et al.* 2008). A  
77 recent increase in the abundance of mafic enclaves may hint at changes in the magma  
78 mingling dynamics in Phase III (Barclay *et al.* 2010). Phases IV (July 2008 – Jan 2009) and  
79 V (Oct 2009 - Feb 2010) marked a change at SHV: eruptive phase length reduced from years  
80 to months and the average extrusion rate increased (Wadge *et al.* this volume). We present  
81 geochemical, textural and petrological analyses of mafic enclaves from Phase IV and V,  
82 alongside results from fieldwork. This work provides a window into syn-eruptive magma  
83 mingling processes.

84

## 85 **Geological Background**

86 Soufrière Hills Volcano (SHV) is located on the island of Montserrat in the Lesser Antilles  
87 island arc. The current eruption at SHV has been ongoing since July 1995 with five phases of  
88 andesitic dome-forming lava extrusion to date (Wadge *et al.* this volume). SHV andesite is  
89 porphyritic (30-40%) and is described in detail in prior studies (Devine *et al.* 1998; Barclay *et al.*  
90 1998; Murphy *et al.*, 2000; Couch *et al.* 2000; Humphreys *et al.* 2009). The phenocryst  
91 assemblage is plagioclase + hornblende + orthopyroxene + Fe-Ti oxides and minor quartz  
92 and rare zircon crystals, whereas the groundmass assemblage is plagioclase + orthopyroxene  
93 + clinopyroxene + Fe-Ti oxides, and interstitial glass is rhyolitic in composition. The andesite  
94 temperature, as bracketed by quartz and amphibole stability is ~830-870 °C (Barclay *et al.*

1998). Within the andesite at SHV mafic enclaves have been ubiquitous (Murphy *et al.* 1998, 2000; Harford *et al.* 2002; Barclay *et al.* 2010 ). Geochemically, SHV andesite compositions have been modelled as the result of fractional crystallisation of equal proportions of amphibole and plagioclase from the South Soufrière Hills basalt (erupted in the south of the island, ~130Ka; Zellmer *et al.* 2003; Harford *et al.* 2002). The SHV mafic enclaves and the South Soufrière Hills basalt are geochemically distinct with different REE trends and are not related by crystallisation (Zellmer *et al.* 2003).

The presence of mafic enclaves in SHV andesite is ascribed to the interaction between mafic magma and the andesitic host magma, which is perhaps the trigger and driver for the current eruption (Devine *et al.* 1998; Murphy *et al.* 1998; Murphy *et al.* 2000; Couch *et al.* 2001). It has been proposed that the initial intrusion of mafic magma underplated the andesitic magma (Murphy *et al.* 2000). A strong viscosity contrast exists between the highly crystalline andesite magma and phenocryst-poor mafic magma, so mechanical mixing is likely to be inhibited significantly (Sparks *et al.* 2000). Enclaves may have formed when fragmented dykes and blobs of less dense mafic material were injected into the overlying andesite (Murphy *et al.* 2000). The remobilisation of the andesitic magma may have taken place via initial conduction of heat across the mafic-andesite boundary followed by the development of instabilities and convection in the andesitic magma (Couch *et al.* 2001). An alternative model suggests that the remobilisation of the andesite (essentially a crystal mush) takes place by ‘gas sparging’, involving the upward migration of a hot fluid volatile phase derived from the mafic intrusion (Bachmann & Bergantz 2006). This fluid transports heat by advection, which is more efficient over shorter time-scales than conduction and may occur alongside limited mafic-silicic mingling, making this model consistent with observations of ‘cryptic’ mafic component of ~6% by volume in Phase III products (Humphreys *et al.* 2009; in press) and of excess gas (Edmonds *et al.* this volume).

Questions still remain concerning the dynamics of the mingling between the two magmas at SHV. Although different enclave types have been recognised in an earlier eruptive phase (Barclay *et al.* 2010), there has been little attempt to decipher the differing petrological and textural features between types. Prior work on enclave petrology has focussed predominantly on Phases I to III. Eruptive phase length has altered in Phases IV and V (Wadge *et al.* this volume), and therefore an additional aim of the work is to evaluate any changes in enclave petrology relative to the early stages of the eruption that might allow us to infer changes in magma reservoir conditions.



128

129 **Methods**

130 Samples of andesite and mafic enclaves were collected from a wide range of locations around  
131 SHV from deposits emplaced during Phase V activity (Table 1). Samples collected from the  
132 February 11<sup>th</sup> 2010 dome collapse deposits in the Trant's area are likely to have originated  
133 from a combination of Phase III, IV and V domes. Although minor Phase III deposits were  
134 incorporated into the collapse (Stinton *et al.* this volume), the distinctive Phase III lava  
135 described by Barclay *et al.* (2010) is inferred only to be a minor component of the flow  
136 deposits based on field observations. The significantly larger extruded volume in Phase V  
137 ( $\sim 74 \times 10^6 \text{ m}^3$ ; Stinton *et al.* this volume) compared to Phase IV ( $\sim 39 \times 10^6 \text{ m}^3$ ; Wadge *et al.*  
138 this volume), implies that many of the samples collected from the February 11<sup>th</sup> dome  
139 collapse were derived from Phase V. Samples that were collected from pyroclastic flow  
140 deposits in Aymers and White River are derived from Phase V (Stinton *et al.* this volume).  
141 Pumice was sampled from across Phase V activity (Oct 2009 – Feb 2010). Phase IV samples  
142 are from the January 3<sup>rd</sup> 2009 vulcanian explosion (Table 1).

143 *Estimation of macroscopic enclave volume fraction*

144 Enclave abundance was estimated using both macroscopic point counting and image analysis  
145 in the Phase V deposits. Nine lava blocks from the February 11<sup>th</sup> 2010 dome collapse  
146 deposits in the Trant's and Streatham areas (see map: Wadge *et al.* this volume) were  
147 analysed using both methods. Selection of the blocks was random, apart from requiring a  
148 relatively exposed and flat surface for analysis. Furthermore, to assess potential anisotropy in  
149 enclave fabric or abundance, two faces of a single block were analysed. For macroscopic  
150 point counting a grid of  $1 \text{ m}^2$  with 2 cm intervals on each axis (Fig. 1b) permitted us to count  
151 up to a total of 2601 points per site. Spacing interval was chosen on the basis of the average  
152 size of enclaves, most are  $< 10 \text{ cm}$  in diameter (Fig. 2). The minimum size of enclaves  
153 counted was 1 cm (smaller enclaves could not be distinguished from crystal  
154 clots/glomerocrysts in the field). In addition to enclave abundance the size and shape of  
155 enclaves were also measured. Using photographs of the same  $1 \text{ m}^2$  area, enclaves were  
156 isolated digitally from the andesite using ImageJ software. The isolated area fraction  
157 occupied by the enclaves was then calculated and compared to the point counting results.  
158 Image analysis yielded similar percentages, but consistently a little lower in comparison to  
159 the point counting method (by a mean of 1%). The slight underestimation of the image

160 analysis method is due to our inability to resolve the small enclaves (<2 cm) in the images,  
161 but is within standard error. We refer to the values obtained by the point counting method for  
162 enclave abundances.

163

#### 164 *Laboratory Analytical Methods*

165 Seventy-four mafic enclaves and andesite samples from Phases IV and V were crushed and  
166 powdered for X-Ray Fluorescence (XRF) analysis to determine major and trace element  
167 concentrations at the University of East Anglia using a Bruker AXS S4 Pioneer. Standard  
168 deviations are <1% for all major oxides, apart from MgO and P<sub>2</sub>O<sub>5</sub>, which are <2%. Trace  
169 element accuracy is <2%, apart from Sc and Ce at <7% and <4% respectively. The diameters  
170 of enclaves analysed ranged from 3.3- 23.8 cm (Table 1). We also analysed different splits of  
171 the same samples, to rule out artefacts resulting from the relatively small sample size.  
172 Standard deviations are <1% for SiO<sub>2</sub>, Al<sub>2</sub>O<sub>3</sub>, P<sub>2</sub>O<sub>5</sub>, Na<sub>2</sub>O and Sr, all other major and trace  
173 element oxides are <5%. However, a single run of sample MT27 did produce anomalously  
174 high standard deviation values for K<sub>2</sub>O and Ba of 15% and 31% respectively. The minimal  
175 deviations seen between different splits of the same sample were not great enough to explain  
176 the range of compositions as also concluded by Zellmer *et al.* (2003).

177 Thin sections of 40 samples were cut from dome rock and pumice. In enclave sections  
178 andesite-enclave margins were included, as well as the interior of large enclaves (>10 cm) to  
179 examine heterogeneity across enclaves. Secondary Electron Microscope (SEM) images were  
180 collected using Jeol JSM-5900LV at University of East Anglia, operating at an accelerating  
181 voltage of 20 kV and a working distance of 10 mm. Electron probe analysis was undertaken  
182 at University of Cambridge using a Cameca 5-spectrometer SX-100 instrument. Major  
183 elements of minerals were analysed using a 15 kV, 10 nA focused beam, and trace elements  
184 using a 15 kV, 10 nA beam. Standard deviations are <0.6% for all major and trace elements.  
185 Glasses were analysed using a 10 µm spot size with a 15 kV, 2 nA and 10 nA beam for major  
186 and trace elements respectively. Standard deviations are <0.9% for SiO<sub>2</sub> and Al<sub>2</sub>O<sub>3</sub>, and  
187 <0.4% for all other major and trace elements.

188 We measured plagioclase phenocryst size, type, and rim and sieve-texture thickness  
189 by analysing representative different enclave types. We used a total of six thin sections, one  
190 type A and the rest type B. We examined a wider range of Type B samples due to a greater

191 degree of heterogeneity across this enclave type. However, we also checked the results  
192 against other type A samples to ensure that there was no bias towards the sample analysed.  
193 We ruled out the possibility of a 2D sectioning of 3D crystals artefact as the overriding cause  
194 of differing rim widths, as we observe a positive correlation between rim width and the  
195 proportion of sieved inherited phenocrysts in different enclaves (see Fig. 3).

## 196 **Results**

197 The andesite erupted in Phase V of the eruption is porphyritic with a fine-grained  
198 groundmass, and contains mafic enclaves as in earlier phases (Fig. 1) (Murphy *et al.* 1998,  
199 2000; Harford *et al.* 2002; Barclay *et al.* 2010). Some andesite blocks contain distinctive  
200 streaked highly crystalline layers of amphibole and plagioclase. Pumice is porphyritic with a  
201 fine-grained groundmass and often contains mafic enclaves.

202 Total measured mafic enclave abundances within andesitic Phase V blocks range  
203 from 2.9% to 8.2% from point counting, with a mean of 5.6% (Table 2). The size of  
204 individual enclaves ranges from 1 to 80 cm; however, ~95% of the enclaves were <10 cm in  
205 apparent diameter (Fig. 2). We categorised Phase V enclaves into three broad types that were  
206 readily identifiable in the field using characteristics such as phenocryst proportions, the  
207 nature of the margin between enclave and andesite, vesicularity, enclave size and shape, and  
208 groundmass size and colour (Table 3). The classification scheme applied by Barclay *et al.*  
209 (2010) is insufficient to describe the large textural diversity of the Phase V enclaves.

210 Type A enclaves are characterised as phenocryst-poor, vesicle-rich, with dark grey  
211 groundmass and chilled margin (Table 3, Fig. 1). In the field these enclaves are readily  
212 identified by their dark grey colour caused by the fine-grained groundmass composition.  
213 Type A enclaves are typically ellipsoidal to sub-angular in shape, with occasional fingers of  
214 the enclave material protruding into the andesite. Commonly the smaller (1-5 cm) angular  
215 enclaves without evident chilled margins are clustered, suggesting that they are fragments of  
216 a larger enclave that disaggregated mechanically after formation. Type A enclave volume  
217 fraction reaches 46 % (with a mean of 22 %) of the total number of enclaves measured (Table  
218 2). These have the smallest mean diameter of all the enclave types measured (2.3 cm),  
219 although large enclaves over 18 cm were also measured (Fig. 2).

220 Type B enclaves are characterised as phenocryst-rich, vesicle-poor, with a light grey  
221 groundmass and indistinct margins (Table 3, Fig. 1). In the field, type B enclaves are a lighter

222 grey than type A, and resemble most closely the host andesite in colour and texture (Fig. 1).  
223 They are generally ellipsoidal and well-rounded, although a few (<5 %) are angular in shape.  
224 Type B enclaves dominate across most of the analysed blocks, and represented 31% to 100%  
225 (with a mean of 64%) of the total enclaves measured. Their size distribution is strongly  
226 positively skewed from the norm with most <6 cm, (with a mean of 3.4 cm; Fig. 2).

227 Type C enclaves are composite and are characterised by distinct textural zones akin to  
228 types A and B (Table 3). Type C enclaves were present in all blocks examined except for  
229 block 5, with variable abundances of 0-41% (mean; 14%; Table 2). The size distribution of  
230 type C enclaves shows a weaker positive skew from the norm towards smaller sizes, (with a  
231 mean of 4.4 cm; Fig. 2). Below 2 cm composite textures were difficult to identify, which may  
232 be a factor in the increased mean size in comparison to other enclave types.

233 Distribution of enclaves is not even through the blocks; enclaves tend to cluster  
234 together, particularly in the smaller size fractions. Heterogeneity is observed both between  
235 blocks and within a single block; *e.g.* for block 1a-b, where two faces of the same block were  
236 measured, block 1a had a lower abundance of enclaves (3.5%), relative to the other face,  
237 block 1b (6.1%, Table 2). Furthermore, type A was absent from block 1a, but type A enclaves  
238 constituted 30% of the total in block 1b (Table 4), and of those, 66% were <2 cm (Fig. 2).  
239 This suggests localised clustering both of enclaves and enclave types.

#### 240 ***Petrological and Textural Analysis***

241 Following the criteria set out in Murphy *et al.* (2000), the term phenocrysts is used for  
242 crystals with major axis >300  $\mu\text{m}$ , microphenocrysts 100-300  $\mu\text{m}$ , and microlites <100  $\mu\text{m}$   
243 for the andesite and enclaves. The compositions of minerals from Phase V andesite are  
244 similar to those from earlier eruptive phases and there is no major change in andesite  
245 assemblage (Murphy *et al.* 2000; Humphreys *et al.* 2009). Mafic enclaves have a diktytaxitic  
246 groundmass framework of elongate, randomly-oriented crystals (Fig. 1d). This groundmass  
247 consists of plagioclase  $\pm$  clinopyroxene  $\pm$  high-Al-amphibole  $\pm$  orthopyroxene. Fe-Ti oxides  
248 are observed throughout, and are often more abundant near inclusion margins.  
249 Titanomagnetite is the most common oxide, but ilmenite is also present. Trace amounts of  
250 apatite are often observed as inclusions in titanomagnetite and plagioclase-inherited  
251 phenocrysts (see below). Variable amounts of interstitial rhyolitic glass (71-78 wt% SiO<sub>2</sub>) are  
252 found within the enclaves. Clinopyroxene (Mg# ~75) occurs as either the breakdown product

253 of amphibole, or as reaction rims on inherited orthopyroxene phenocrysts, or in the  
254 groundmass of the inclusions. The degree to which the framework is interlocked is usually  
255 correlated negatively with the amount of glass, disruption of vesicles and sizes of the  
256 groundmass crystals.

257 Large crystals (~2-3 cm) of plagioclase, amphibole and orthopyroxene are present in  
258 the mafic enclaves (Fig. 1d); most exhibit textural and compositional evidence that they have  
259 been inherited from the andesite (Murphy *et al.* 2000; Humphreys *et al.* 2009). We refer to  
260 these as inherited phenocrysts as they are not antecrystic or xenocrystic in origin. Following  
261 Murphy *et al.* (2000), the large inherited plagioclase phenocrysts in the enclaves can be split  
262 into two main types. Type 1 comprise large oscillatory zoned sodic phenocrysts (An<sub>49-57</sub>) with  
263 calcic rims (An<sub>69-80</sub>) 40-47 µm thick, similar to the type 1 and 2 plagioclases in the andesite  
264 (after Murphy *et al.* 2000). Type 2 are reverse-zoned dusty sieve-textured phenocrysts, where  
265 the sieve-texture (of thickness 70 µm to extending to the crystal core) is overgrown by a clear  
266 calcic rim (of thickness 0-230 µm) and comprises glass and high-anorthite (An<sub>70-90</sub>)  
267 plagioclase. Smaller crystals (<1000 µm) have a pervasive sieve-texture. Rim width is  
268 typically largest where the degree of sieve texture is highest (Fig. 3). Low anorthite  
269 compositions (An<sub>49-57</sub>) of the cores in both plagioclase types are identical to andesite  
270 phenocrysts compositions observed throughout the eruptive phases (Murphy *et al.* 2000;  
271 Humphreys *et al.* 2009). Core-to-rim transects across inherited plagioclase phenocrysts show  
272 a sharp increase in X<sub>An</sub>, FeO and MgO at the rim. Inherited amphibole phenocrysts are Mg-  
273 hornblende (Leake *et al.* 1997), identical to low Al<sub>2</sub>O<sub>3</sub> (6-8 wt %) amphiboles phenocrysts in  
274 the andesite. They are often variably opacified, or partially reacted, with plagioclase and  
275 clinopyroxene overgrowths, indicating instability due to heating, rapid decompression or  
276 shallow storage in the dome (Garcia & Jacobson 1979; Murphy *et al.* 2000; Rutherford &  
277 Devine 2003; Browne & Gardner 2006; Buckley 2006; Plechov *et al.* 2008). Inherited  
278 orthopyroxene phenocrysts commonly have clinopyroxene overgrowths, Fe-Ti oxide  
279 inclusions, are typically reverse-zoned, with Mg# 58-74 identical to the andesite  
280 orthopyroxene compositions (Murphy *et al.* 2000; Humphreys *et al.* 2009). Rare embayed  
281 quartz phenocrysts with rims of clinopyroxene were also observed. Rare zircon crystals are  
282 also present in some enclaves.

283 *Type A Enclaves*

284 In thin section, type A enclaves (Table 3 and Fig. 4) are defined by a fine-grained  
285 groundmass, high vesicularity (19-40%, Fig. 5), chilled margins and low abundance of  
286 inherited phenocrysts (0 – 8.6%, Table 4, Fig. 6). The framework consists predominantly of  
287 plagioclase, with acicular amphibole and clinopyroxene also present. In the framework  
288 plagioclase disequilibrium features similar to a sieve texture can be seen developing in the  
289 cores of many microphenocrysts. These are enclosed by rims of clear plagioclase of  
290 composition  $An_{77-89}$  (Table 5, Fig. 4d). The framework amphibole (~13-15 wt %  $Al_2O_3$ ,  
291 Table 5) is magnesio-hastingsite to pargasite (Leake *et al.* 1997), and typically has reaction  
292 rims of clinopyroxene that range from 5  $\mu m$  thick to sometimes pervading the entire crystal  
293 (Fig. 4e). In Phase I the presence of framework amphibole was interpreted to correspond with  
294 larger enclave sizes (Murphy *et al.* 2000); this appears not to be the case in Phase V.  
295 Framework amphibole is present irrespective of the size of the enclave. Glass abundance is  
296 low (<5%), but is concentrated near vesicles and chilled margins. It contains on average 75wt  
297 %  $SiO_2$  and 3.8 wt %  $K_2O$  (Table 5 and Fig. 7). Chilled margins are typically present, defined  
298 by a decrease in groundmass grain size towards the boundary, which is sharp to weakly  
299 gradational. Across large enclaves, inherited phenocryst abundances can be spatially  
300 extremely variable with densely clustered plagioclase phenocrysts associated with regions of  
301 increased enclave vesicularity. Type 1 plagioclase (with minor disequilibrium textures) is  
302 usually absent with predominantly type 2 (sieve-textured) dominating (Table 4). The rims on  
303 type 2 crystals range from 132–230  $\mu m$  thick, which are the thickest rims measured in all the  
304 enclave types (Fig. 3). The rims of the inherited phenocrysts have high anorthite contents, of  
305  $An_{80-90}$  (Table 5). Inherited amphibole phenocrysts are commonly completely opacified  
306 with very little amphibole remaining, or have been almost completely replaced by  
307 clinopyroxene and plagioclase reaction products. Inherited phenocrysts are rarely observed  
308 transecting the boundary in this enclave type.

309

### 310 *Type B Enclaves*

311 Type B enclaves (Table 3 and Fig. 8) are defined by a variably sized fine to medium-grained  
312 groundmass, low to medium vesicularity (9-19%, Fig. 5), diffuse margins, and medium to  
313 high inherited phenocryst abundance (16.5-26%, Fig. 6 and Table 4). As with all enclave  
314 types the framework is predominantly plagioclase ( $An_{65-75}$ ), which have lower  $X_{An}$  values in  
315 comparison with type A framework-phase plagioclase ( $An_{77-89}$ ). High-Al framework

316 amphibole is typically absent, but occasionally present in enclaves with lower abundances of  
317 inherited phenocrysts (*i.e.* those that are closest to the type A enclaves). Glass is rare (<5%),  
318 and contains on average 77 wt% SiO<sub>2</sub> and 2.9 wt% K<sub>2</sub>O (Table 5; Fig. 7), and is typically  
319 pooled near large vesicles where present. Orthopyroxene microlites (Wo<sub>2-4</sub>, Fs<sub>38-40</sub>, En<sub>56-60</sub>,)  
320 and calcic plagioclase microlites are sometimes observed growing outwards from vesicle  
321 walls (Fig. 8c). Some enclaves have large elongated vesicles, (~4 cm) with some vesicles  
322 disrupting the diktytaxitic framework, where crystals close to larger vesicles appear to have  
323 been bent after formation. Crystals (microlites or inherited phenocrysts) are regularly seen  
324 transecting enclave margins (Fig. 8). Type 2 inherited plagioclase phenocrysts dominate  
325 (Table 4); overall rim thickness (27-113 μm) is smaller in comparison to type A enclaves (see  
326 above) and is variable between different enclaves (Fig. 3). Inherited amphibole phenocrysts  
327 have variable disequilibrium textures: phenocrysts are either completely opacified, broken  
328 down to clinopyroxene and plagioclase, or have undergone only minor disequilibrium. Rare  
329 inherited quartz with clinopyroxene overgrowth rims are also observed.

330

### 331 *Type C Enclaves*

332 Type C enclaves are composite, with at least two distinct different textural zones with respect  
333 to colour, vesicularity, and inherited phenocryst assemblage. Sample MT08 for example has a  
334 dark grey interior surrounded by a lighter grey exterior (Fig. 8e-f). The dark grey interior is  
335 somewhat similar to the type A enclaves, with a diktytaxitic groundmass framework  
336 composed of plagioclase (~An<sub>84</sub>, Table 5), amphibole (~14 wt % Al<sub>2</sub>O<sub>3</sub>, Table 5) and  
337 clinopyroxene, and a mean vesicularity of 23.9%. Inherited phenocryst abundance is low  
338 (12.6%); type 2 inherited plagioclase phenocrysts are dominant. The lighter grey outer  
339 portion resembles type B enclaves, with a diktytaxitic framework of plagioclase (~An<sub>72</sub>) and  
340 clinopyroxene; this portion does not display the same degree of crystal interlocking as the  
341 darker interior portion. Sparse high-Al amphibole laths are also observed in the outer portion  
342 close to the margin with the interior portion, typically where the margin is more diffuse.  
343 Furthermore, at the most diffuse margins plagioclase microphenocrysts are often observed.  
344 Vesicularity is lower in the outer portion relative to the interior portion (17.2%). Inherited  
345 phenocryst abundances are high (26.5%), dominated by plagioclase type 2, but type 1 is also  
346 present. Inherited amphibole and orthopyroxene are also present, which typically display  
347 more subtle disequilibrium textures than in the interior portion. The glass fraction is between

348 5 and 10%, and it is higher in the interior portion. Glass composition is similar to the type B  
349 enclaves in both portions, although the interior portion has slightly lower mean (74 wt%  
350 SiO<sub>2</sub>) to the exterior (75 wt% SiO<sub>2</sub>; Table 5, Fig. 7). The margin between the exterior portion  
351 and the host andesite is diffuse, with phenocrysts transecting the margin.

### 352 *Enclaves In Pumice*

353 Enclaves in pumice are extremely vesicular compared to those in lava dome blocks. The  
354 margins of the enclaves are lined with large coalesced vesicles, inhibiting identification of the  
355 original (pre-decompression) margin texture. Large amphiboles in the enclaves sometimes  
356 display boudinage textures similar to those seen in the andesite pumice (Giachetti *et al.*  
357 2010). We do not include enclaves in pumice in our classification scheme owing to the large  
358 degree of textural overprinting of features by late-stage ascent processes.

### 359 **Geochemistry**

360 We present whole rock major and trace element geochemical data for the mafic enclave types  
361 discussed above and andesite from Phases III, IV and V, and examine geochemical  
362 differences between the enclave types, as defined on the basis of their texture and petrology.

363 We first compare phases IV and V major and trace element composition with the  
364 earlier phases of the eruption. Phases IV and V mafic enclaves and host andesite continue to  
365 fall on the linear array of most major elements, as established in previous phases (Fig. 9)  
366 (Murphy *et al.* 2000; Zellmer *et al.* 2003). Although phase V andesite SiO<sub>2</sub> is slightly lower  
367 on average than earlier phases, values still lie within the range of data from the previous  
368 phases (Fig. 9). However, the compositional gap in SiO<sub>2</sub> between the mafic enclaves and the  
369 andesite observed in phases I-III, no longer exists in phase V (Fig. 9). Phase V andesite and  
370 mafic enclaves do not continue the trend of increasing MgO and decreasing Fe<sub>2</sub>O<sub>3</sub> established  
371 between Phases I to III (Barclay *et al.* 2010) (Fig. 9), but instead remain similar in  
372 composition to Phase III.

373 The different categories of enclaves, as defined by their textural and petrological  
374 features, are also distinct in terms of bulk geochemistry. Although the type A and B enclaves  
375 fall on a single linear array with the andesite with no compositional gaps, each type plots in a  
376 distinctive field for all major elements (Fig. 10). Type A enclaves occupy a narrow  
377 compositional range (49.7-52.4 wt % SiO<sub>2</sub>), whereas type B enclaves have a much broader  
378 range (53-58 wt% SiO<sub>2</sub>) (Fig. 10). Trace element distributions in the enclaves studied are



379 consistent with previous studies. For example, Zr is positively correlated with SiO<sub>2</sub>, whilst V  
380 is negatively correlated (Fig. 10). Type A enclaves have systematically higher compatible  
381 trace element contents, and lower incompatible trace element contents, than the type B  
382 enclaves (Fig. 10).

383 In the composite Type C enclaves, interior portions are less evolved (52.7 to 55.4  
384 wt% SiO<sub>2</sub>) and the outer portions are more silicic (55.8 to 58.1 wt % SiO<sub>2</sub>), with one point  
385 lying in the host andesite field. The relative difference between the two portions is typically  
386 about 3 wt %, irrespective of absolute SiO<sub>2</sub> values. However, Type C enclave bulk  
387 compositions plot entirely within the field for Type B enclave points (Fig. 10).

388 Glass compositions are rhyolitic (71-79 wt % SiO<sub>2</sub>, Table 5) for the mafic enclaves  
389 similar to prior eruptive phases and lie within established trends (Humphreys *et al.* 2010;  
390 Murphy *et al.* 2000). There are some notable differences between the enclave types of Phase  
391 V. Type A enclaves have a wide scatter of K<sub>2</sub>O compositions in comparison to types B and  
392 C, but is higher on average (Fig. 7a). Type A enclaves also have on average higher FeO and  
393 MgO (Fig. 7b). In contrast type B enclaves have low FeO and MgO compositions. Type C  
394 inner and outer enclave portions glass compositions were measured. In most elements  
395 measured there is an observed difference between the two portions. The inner portion  
396 compositions plot within the type A field in FeO, MgO and TiO<sub>2</sub>, whereas the outer portion  
397 compositions tend to plot within the type B field in K<sub>2</sub>O (Fig. 7a). There are however  
398 considerable overlap between the fields in FeO and MgO (Fig. 7b).

### 399 **Summary**

400 In summary we find that there are distinctive textural, petrological and geochemical  
401 differences between the phase V enclave types (Table 3). Type A enclaves are least evolved  
402 with a narrow compositional range, a low inherited phenocryst fraction, high vesicularity and  
403 with chilled margins. Type B enclaves have a broader, but more silicic compositional range, a  
404 high inherited phenocryst fraction and no chilled margins. The composite Type C enclaves  
405 have a more mafic inner portion with an affinity to type A, and an outer more silicic portion  
406 akin to Type B. We examine the constraints on the formation of the differing enclave types to  
407 help constrain a model of the mingling dynamics between the andesitic and mafic magmas in  
408 Phase V.

409

410 **Discussion**

411 In general, the low crystallinity and inherited phenocryst content, chilled margins, and  
412 relatively restricted primitive geochemical composition suggests that the type A enclaves are  
413 close to an end-member mafic magma that quenched rapidly on contact with the andesite. In  
414 contrast, type B enclaves, with their much higher inherited phenocryst content, lack of chilled  
415 margins and more evolved compositions, are significantly hybridised. Type C enclaves are  
416 composite, with a more mafic interior indicating dynamic mingling between types A and B.  
417 Below we discuss in detail the constraints on the formation of these three enclave types and  
418 implications for the nature of magma mixing at Soufrière Hills Volcano.

419

420 ***Geochemical constraints on end-member magma compositions***

421 Work by Zellmer *et al.* (2003) indicates that the mafic magma is formed by closed-system  
422 fractional crystallisation of amphibole (70%) and plagioclase (30%). The type A enclaves are  
423 the least evolved of the enclave types, with low incompatible trace element concentrations;  
424 we therefore interpret them to be closest to a hypothesised low SiO<sub>2</sub> mafic magma end-  
425 member. However, the presence of inherited phenocrysts indicates that even these least  
426 evolved enclaves are already hybridised.

427 The Type B enclaves are more evolved in comparison to type A, but reflect a broad  
428 range of compositions. The strongly linear compositional arrays in major elements (Al<sub>2</sub>O<sub>3</sub>,  
429 CaO *etc.*) and trace elements (Zr, Ba *etc.*) through the mafic enclaves to the host andesite in  
430 Phase V (Fig. 10), supports a mixing relationship between the mafic and andesite end-  
431 members. This suggests that type B enclaves reflect a continuum of degrees of mixing.  
432 Nonetheless, we also observe that there is bimodal distribution between the total inherited  
433 phenocryst fraction between types A and B. Using the average core compositions of  
434 inherited plagioclase and amphibole phenocrysts, we find that addition of the phenocrysts to  
435 the mafic melt should drive the melt to more mafic compositions (Fig. 10). However, the  
436 trend between Type A and B is towards more evolved compositions with increasing  
437 phenocryst abundance (Fig. 6), suggesting that the phenocryst incorporation has relatively  
438 little impact on bulk composition and that mixing is the dominant process.

439 The relatively homogeneous rhyolitic composition of glass in the mafic enclaves could  
440 indicate that felsic melt from the andesite has infiltrated into the mafic enclaves, or may

441 simply be the result of extensive crystallisation of a mafic melt. Engulfment of inherited  
442 phenocrysts must also be accompanied by liquid assimilation from the andesite host, which  
443 will affect the bulk composition of the mafic enclaves. If this is the case, type B melt  
444 compositions may reflect a localised hybrid starting composition before framework  
445 crystallisation in contrast to the type A melt. At Narugo Volcano, Japan compositional  
446 similarity between glasses in the host magma and mafic inclusions is interpreted as evidence  
447 of infiltration of the host magma melt into a boundary layer before enclave formation (Ban *et*  
448 *al.* 2005). Although glass compositions of the andesite and enclaves are both rhyolitic and  
449 overlap at SHV, there is a clear difference between the types A and B glass in K<sub>2</sub>O (Fig. 7a).  
450 Type B is somewhat similar to the andesite (Humphreys *et al.* 2010) and less variable than  
451 type A glass. This may imply that the melt in Type B enclaves is more homogenised in  
452 comparison to Type A allowing K<sub>2</sub>O time to re-equilibrate with the andesite host (Humphreys  
453 *et al.* 2010). The diffusive timescale of K has been calculated to be 32 days for rhyolitic  
454 compositions across a length-scale of 1 cm (Humphreys *et al.* 2010). Therefore, preservation  
455 of the higher K<sub>2</sub>O glass composition of the type A enclaves may be attributed to a shorter  
456 timescale of mixing than type B.

457

#### 458 ***Petrological and textural mingling constraints***

459 The presence of chilled margins, lower inherited phenocryst abundance, higher plagioclase  
460 anorthite compositions and ubiquitous presence of high Al-amphibole in the framework  
461 crystals of type A enclaves relative to the type B enclaves all suggest that controls on the  
462 formation differed between the enclave types.

463 Engulfment of phenocrysts from the host magma by an incoming magma has been  
464 observed elsewhere *e.g.* Unzen, Kameni, Chaos Craggs (Clynne 1999; Browne *et al.* 2006a;  
465 Martin *et al.* 2006a; Feeley *et al.* 2008). Previous work on inherited plagioclase phenocrysts  
466 from SHV demonstrates a positive correlation between iron and anorthite content at the  
467 phenocryst rim (Humphreys *et al.* 2009). The disequilibrium textures and rim growth on the  
468 plagioclase was therefore probably caused by the incorporation of the inherited phenocrysts  
469 into a high-calcium melt (Ruprecht & Wörner 2007; Humphreys *et al.* 2009) rather than by  
470 decompression and degassing (Coombs *et al.* 2000). The presence of inherited phenocrysts in  
471 the type A enclaves, where chilled margins would significantly inhibit mass exchange  
472 between the enclave and andesite (Blake & Fink 2000), indicates that the majority of

473 phenocryst incorporation must have taken place before chilled margin formation. The higher  
474 inherited phenocryst fraction in the type B enclaves (16.5-26%) in comparison to the Type A  
475 enclaves (0 – 8.6%) indicates a greater interaction with the andesitic melt prior to enclave  
476 formation (Fig. 6). Differing rim and sieve-texture disequilibria widths of the inherited  
477 plagioclase phenocrysts in individual enclaves may reflect differing time-scales of  
478 engulfment or conditions of residence in the mafic melt (Fig. 3). In contrast, at Unzen, Japan,  
479 uniformity of calcic rim widths and sieve-textures of inherited plagioclase phenocrysts are  
480 interpreted as indication of a single episode of engulfment of phenocrysts into enclaves  
481 (Browne *et al.* 2006b).

482         The effect of adding inherited phenocrysts on the viscosity of the mafic magma was  
483 estimated using the Einstein-Roscoe relation for effective viscosity, with melt viscosity  
484 calculated using the empirical model of Giordano *et al.* (2008). We find that the addition of  
485 the inherited phenocrysts increases the effective viscosity of the mafic magma and dominates  
486 over the effect that the associated temperature reduction would have (Fig. 11). However, even  
487 with the maximum observed volume of 25 % inherited phenocryst fraction in the type B end-  
488 member a relative viscosity contrast between the andesite (45-55 vol% phenocrysts) still  
489 exists. Prior to mafic magma crystallisation, the viscosity will be lower than the andesite  
490 viscosity. However, after quench crystallisation, where crystal content can be >90% vol,  
491 enclave viscosity will be greater than andesite viscosity and this will inhibit mixing (Sparks  
492 & Marshall 1986). The inherited phenocryst content also contributes to a viscosity contrast  
493 between types A and B, which implies that mixing would be inhibited between the two types  
494 (Fig. 11).

495         The diktytaxitic framework observed in both type A and B enclaves demonstrate that  
496 quench crystallisation took place during thermal equilibration with the andesite. This implies  
497 that a temperature contrast must exist between the andesite and even the most hybridised  
498 mafic melt prior to enclave crystallisation. However, textural and petrological differences  
499 show that this contrast was variable during formation of types A and B enclaves. An overall  
500 higher anorthite content of type A enclave inherited plagioclase phenocryst rims,  
501 microphenocrysts and microlites in comparison to type B enclaves, could be indicative of  
502 crystallisation under hotter conditions or more H<sub>2</sub>O-rich conditions. Differing sized enclaves  
503 and types may take different times to equilibrate thermally (Bacon 1986), and therefore  
504 phenocryst disequilibrium is likely to be slightly different between enclaves. However,  
505 inherited plagioclase phenocrysts' sieve-textures and rims in type A enclaves are consistently

506 thicker (Fig. 3). This hints at higher temperatures, rather than a longer residence time of the  
507 inherited phenocrysts in comparison to type B enclaves, which may be consistent with  
508 inferences from the residual glass composition. Furthermore, this process would be limited by  
509 the rapid cooling that would take place as the enclave reached thermal equilibrium (Bacon  
510 1986; Sparks & Marshall 1986). Chilled margins reflect rapid cooling caused by a significant  
511 temperature contrast between the enclave and host magma, with the enclave largely liquid  
512 during formation (Bacon 1986; Sparks & Marshall 1986; Clyne 1999). We therefore infer  
513 that type A enclaves not only formed from a hotter melt than type B, but that formation was  
514 the result of injection into the andesite as a liquid, where rapid cooling drove crystallisation  
515 and formation of the chilled margins.

516         The lack of chilled margins in type B enclaves could result either from a smaller  
517 temperature contrast between enclave and andesite, in comparison to type A, or from  
518 mechanical abrasion of enclave margins caused by shear stress (Feeley & Dungan 1996). We  
519 suggest that mechanical abrasion would be unlikely to remove all evidence of a chilled  
520 margin. A reduced temperature contrast would prevent strong decrease in crystal size at the  
521 chilled margin, and allows greater time for mass and chemical exchange during quenching  
522 (Bacon 1986). A temperature contrast of 15-50 °C has been experimentally constrained to  
523 produce similar textures to the type B enclaves during crystallisation in a layer at the silicic-  
524 mafic interface (Coombs *et al.* 2002). Furthermore, variability in textures in the type B  
525 enclaves may be a function of crystallisation depth below a mafic-silicic interface, as slower  
526 cooling will take place further away from the boundary (Coombs *et al.* 2002; Martin *et al.*  
527 2006a). This may indicate that quench crystallisation of the type B enclaves took place  
528 before incorporation into the andesite and subsequent disaggregation (*e.g.* Eichelberger  
529 1980; Martin *et al.* 2006a).

530         The ubiquitous presence of the high-Al amphibole laths in the type A as opposed to  
531 the type B enclaves might be a function of melt volatile content. In several plutonic centres  
532 such as the Cadillac Mountain Granite and the Pleasant Bay Intrusion, a positive correlation  
533 between more hybridised (higher SiO<sub>2</sub>) enclaves, with the absence of hornblende and  
534 presence of clinopyroxene has been observed (Wiebe 1993; Wiebe *et al.* 1997). The change  
535 from a hydrous to anhydrous assemblage is attributed to the exchange of H<sub>2</sub>O between stably  
536 stratified mafic and silicic layers (Wiebe *et al.* 1997). Amphibole compositions in the type A  
537 enclaves have 6.4-9.0 wt % H<sub>2</sub>O calculated using the method of Ridolfi and Renzulli (2011).  
538 This is consistent with RhyoliteMelts modelling of a saturated water-rich mafic magma (>8

539 wt % H<sub>2</sub>O), which reproduces the observed porosity and fraction of melt remaining in the  
540 type A enclaves (Edmonds *et al.* this volume). The lower porosity and abundance of  
541 amphibole in the type B enclaves might suggest a lower melt volatile content in comparison  
542 to type A. The presence of some high-Al amphiboles laths in the least evolved type B  
543 enclaves implies that the H<sub>2</sub>O content was sufficient to allow limited amphibole  
544 crystallisation. Variability in the volatile content of the mafic magma might be also account  
545 for differences in the anorthite content of the plagioclase microphenocrysts between enclave  
546 types. Higher H<sub>2</sub>O melt content can lead to higher anorthite content as opposed to just higher  
547 temperatures, which is consistent with the type A enclaves (*e.g.* Couch *et al.* 2003b).  
548 Alternatively, the high-Al amphibole might have had more time in the type B enclaves to  
549 resorb, which also might explain their absence.

550         The plagioclase framework microphenocryst disequilibria observed in the type A  
551 enclaves (Fig. 4c) could be created by a number of processes; (1) strong undercooling where  
552 melt is trapped in the skeletal structure of the crystals as they grow rapidly (2)  
553 decompression-induced disequilibria (Nelson & Montana 1992) (3) degassing-induced  
554 disequilibria (Frey & Lange 2011). As there is already evidence to suggest higher rates of  
555 cooling in the type A enclaves, the large temperature contrast could conceivably be the  
556 controlling process. However, destabilisation of some framework parasitic amphibole rims  
557 indicated by breakdown to clinopyroxene may indicate decompression-induced disequilibria  
558 or shallow storage residence in the dome (Rutherford & Devine 2003; Browne & Gardner  
559 2006; Buckley 2006).

560         The large coalesced vesicles in some of the type B enclaves suggest vesicle expansion  
561 caused by decompression or by longer timescales. Coalesced vesicles have been cited as  
562 evidence of overturn and subsequent breakup of a foam layer at the mafic-silicic interface  
563 (Martin *et al.* 2006a). Bent framework crystals also imply vesicle expansion after  
564 crystallisation (Martin *et al.* 2006a). This disruption to the enclave framework implies that  
565 the type B enclaves are perhaps disaggregated fragments of larger pieces (Martin *et al.*  
566 2006a; Edmonds *et al.* this volume). This is further supported by the presence of clusters of  
567 small angular to sub-angular enclaves within andesite. In a sample of andesite from Phase III,  
568 Humphreys *et al.* (in press) calculated that the total cryptic abundance of material derived  
569 from disaggregation of mafic enclaves is approximately 6-7%, implying that this process is  
570 prevalent at SHV. Microlites or microphenocrysts of high-Al amphibole are very rarely

571 observed within the andesite, which lends support to the idea that it is largely or even  
572 exclusively this hybridised layer that is experiencing this level of disaggregation.

573

#### 574 *Type C Enclaves*

575 Composite or mixed enclaves have been observed in previous eruptive phases (Barclay *et al.*  
576 2010) as well as Phases IV and V. Composite enclaves are suggestive of more complex  
577 hybridisation mechanisms. The inner portion of the enclave used for this study has retained a  
578 compositional and textural identity similar to the more mafic type A. While the surrounding  
579 more silicic portion is texturally and compositionally similar to type B enclaves. The  
580 concentration of glass near the interior margin of the inner part of the enclave, together with  
581 the diktytaxitic framework present, suggests that hotter, more mafic magma is mingled into  
582 the cooler more silicic magma, whilst both are still fluid (Snyder *et al.* 1997). The presence  
583 of a few high-Al amphibole laths in the more silicic portion near the inner margin  
584 demonstrates that there has been limited mechanical exchange of melt and groundmass  
585 material between the two portions of the enclave. The enclave-andesite margin, with fingers  
586 of andesitic material intruding into the enclave indicates weak cooling of the silicic portion in  
587 contact with the host andesite. Composite enclaves may form as mafic magma ‘pillows’,  
588 surrounded by a thin film of hybrid material separating the mafic from the silicic magma  
589 (Blake & Ivey 1986; Snyder *et al.* 1997). The inner mafic portion will crystallise first, and  
590 then the surrounding hybridised portion preserving the interior mafic portion (Collins, 2000).

#### 591 *Phase V mingling model*

592 We propose that the textural and petrological variations of the type A and B enclaves are  
593 created by differing formation mechanisms, partly influenced by the degree of mingling  
594 between the host andesite and intruding mafic magma, which in turn controls temperature and  
595 viscosity contrasts. In addition, the nature and timing of incorporation of the enclaves into the  
596 andesite may also play a role in the differences between the enclaves. In our model for  
597 enclave formation (Fig. 12), volatile-saturated mafic magma is injected into the chamber as a  
598 plume, and mixes with the host andesite to varying degrees, engulfing the andesite-derived  
599 phenocrysts and creating a hybrid mafic magma with a broad range of compositions. Type A  
600 enclaves formed at high rates of cooling and therefore may have formed at the plume margin  
601 (Browne *et al.* 2006a). The high viscosity contrast between the mafic and andesitic magma

602 end-members would prevent effective mixing (Fig. 11), but viscous shearing of the plume  
603 margin could have taken place. Alternatively, blobs of less dense mafic magma might have  
604 detached from the plume during injection into the andesite as a ‘spray’ quenching upon  
605 incorporation into the andesite. Ponding of the intruding magma from plume collapse is likely  
606 to have occurred either as a result of a decrease in the rate of injection (*e.g.* Eichelberger  
607 1980; Sparks & Marshall 1986) or in the density contrast with the andesite (Feeley *et al.*  
608 2008). This leads to the formation of a mafic hybrid layer where at the mafic-silicic interface  
609 crystallisation-induced vesiculation occurred (Eichelberger 1980), from which type B  
610 enclaves are derived (Fig. 12b). For enclave flotation to occur, the H<sub>2</sub>O content of the  
611 enclaves must be >6 wt % (Edmonds *et al.* this volume). Disruption of the mafic-silicic  
612 interface may be result of (1) crystallisation-induced vesiculation, where the density of the  
613 hybrid mafic magma reduced beneath that of the andesite and enabled overturn or (2) an  
614 instability or plume of the mafic magma intruded through the hybrid layers destabilising and  
615 inducing breakup, reproducing the cycle.

616 Composite enclaves may form from small plumes of vesicular, less dense, hotter  
617 mafic material which could buoyantly rise and mingle within the overlying cooler hybridised  
618 layers (Cardoso & Woods, 1999). The compositional and viscosity gap between types A and  
619 B end-members would limit mixing (Fig. 11) and perhaps allow the composite enclaves to  
620 form. These could form undercooled mafic pillows within the hybrid layer, which is then  
621 intruded into the overlying andesite (Fig. 12c). However, this does not explain adequately the  
622 presence of the inherited phenocrysts in the interior more mafic portion of the enclaves.

623 It is unclear if the timing of the processes forming the type A, B and C enclaves are  
624 similar. The presence of the composite enclaves could imply multiple injections of mafic  
625 magma, and suggest a temporal separation between types A and B. Differences in glass  
626 compositions (Fig. 7), also may indicate longer mingling time-scales for the type B enclaves  
627 in comparison to type A. In addition, differing degrees of inherited phenocryst disequilibria  
628 within single enclaves might suggest temporal variations of the engulfment of phenocrysts  
629 rather than a single intrusion. However, as SHV is a long-lived system with multiple  
630 extrusive phases with evidence for quasi-continuous intrusion at depth, it is likely to  
631 demonstrate dynamic mingling. We also cannot rule out that the differing enclave types may  
632 be due to turbulent mingling processes rather than suggesting temporal differences.



633 Finally, we also cannot rule out the possibility that Type A and B enclaves may represent two  
634 separate magmas rather than simply differences in the degree of hybridisation. This is  
635 suggested by the clear differences in inherited phenocryst and vesicle abundances, glass  
636 compositions, and melt volatile contents, although the linear major- and trace-element  
637 compositional arrays do suggest variable hybridisation. The composite enclaves clearly  
638 demonstrate that two-stage mixing has occurred. We might expect to see clear differences in  
639 rare earth elements between the types, if these represent two separate magmas.

640

#### 641 *Comparison with earlier extrusive phases*

642 Observed changes in the eruptive phase length, mafic enclave abundances and bulk  
643 geochemistry lead us to question whether there has been any temporal change in the nature of  
644 the intruding or erupted magma in phases IV and V. The increased average SiO<sub>2</sub> bulk rock  
645 composition of the mafic enclaves since phase III (Fig. 9), together with the dramatic increase  
646 in compositional range of the enclaves (from basaltic to andesitic) (Fig. 9) means that there is  
647 no longer a compositional gap between the mafic enclaves and host andesite. This suggests  
648 that there has been an overall increase in the degree of hybridisation between the mafic and  
649 andesitic magmas in Phases IV and V. Increased hybridisation of the mafic magma could be  
650 related to lower degrees of cooling against the host andesitic magma, perhaps due to  
651 successive replenishments of hotter mafic magma or continued transfer of heat from the  
652 existing mafic source (Wiebe 1993; Wiebe *et al.* 1997; Collins *et al.* 2006; Turnbull *et al.*  
653 2010). The effective viscosity contrast would also be reduced between the two magmas and  
654 thus promote greater mixing between the two magmas, resulting in more hybridised enclaves  
655 as the current eruption continues (Sparks and Marshall, 1986). If this explanation is correct,  
656 continued heating must be relatively localised; otherwise we would anticipate observing  
657 changes to the phenocryst rim compositions in the andesite in phase V, which we do not. We  
658 also expect changes to the crystal size distributions of the mafic enclaves over time, although  
659 this is beyond the scope of the current study.

660

#### 661 **Conclusions**

662 We provide a complete petrological, textural and geochemical description of three distinct  
663 mafic enclave populations in the Soufrière Hills andesite, from the eruptive products of

664 phases IV and V of the current eruption. Type A are basaltic with a narrow range of  
665 compositions, and are recognised by the presence of chilled margins and high-Al amphiboles,  
666 high vesicularity and high inherited phenocryst abundance. Type B have a broad range of  
667 compositions (basaltic andesite), and are identified by a lack of chilled margins, low  
668 vesicularity and high inherited phenocryst abundance, and rare to absent high-Al amphiboles.  
669 Type C are composite with a more mafic interior zone, which is similar to the described type  
670 A, and an exterior zone akin to type B. Analysis of bulk compositions, textures, enclave  
671 petrology and viscosity demonstrates that differences between the enclave types are partially  
672 the result of the degree of mingling between the andesite and mafic magmas. This in turn has  
673 led to differing contrasts in temperature, viscosity, density and composition between the  
674 enclave types. We interpret Type A to be close to a mafic end-member magma, while Type B  
675 is significantly hybridised; Type C represents an interface between the two types.

676 We observe linear compositional arrays between Type A enclaves and the host  
677 andesite; with type B enclaves reflecting a broad range of compositions on these arrays (Fig.  
678 9). In addition, the presence of inherited phenocrysts confirms that all enclaves are hybridised  
679 to some degree. The higher inherited phenocryst abundances in type B indicate a greater  
680 degree of interaction with the host andesite. All enclaves contain rhyolitic matrix glass due to  
681 crystallisation, but there are observable differences in composition between enclave types.  
682 Variations in  $K_2O$  may reflect differing time-scales for mingling and reequilibration between  
683 the enclave types.

684 The absence of the high-Al amphibole, and lower anorthite content of plagioclase  
685 microphenocrysts in the Type B enclaves may be due to a lower melt volatile content in Type  
686 B relative to Type A. The chilled margins in type A enclaves indicate that crystallisation and  
687 formation was driven by rapid cooling with the andesite, while the more hybridised Type B  
688 experienced slower cooling. Differences in degree of mingling probably arise from variations  
689 in temperature, composition and viscosity contrasts between the andesite and mafic magmas.  
690 Thus the distinct textural, petrological and geochemical differences between enclave types  
691 reflect differing formation histories. The more mafic Type A enclaves were formed from an  
692 injected plume of more primitive mafic magma, where limited mingling led to minor  
693 incorporation of inherited phenocrysts. Continued mixing of the intruding mafic magma  
694 resulted in a hybrid mafic magma, which ponded at the base of the chamber. The texturally  
695 broad Type B enclaves represent differing fragments from within a disrupted hybrid layer  
696 formed at the mafic-silicic interface. Composite enclaves represent two-stage mingling

697 between types A and B, where more mafic magma has intruded into the more hybrid magma  
698 layer reflecting temporal differences between them.

699 There is a suggestion that the degree of hybridisation has changed during the course  
700 of the current eruption, as reflected in the disappearance of the SiO<sub>2</sub> gap between the host and  
701 mafic enclaves bulk compositions in Phase V. This could be due to continued mafic  
702 replenishment causing localised reductions in the temperature contrast between the magmas  
703 as heat is transferred from the mafic intrusion to the andesite. This might permit localised  
704 increases in the degree of mixing between the mafic and andesite magmas.

## 705 **Acknowledgements**

706 MP acknowledges the support of a NERC studentship NE/H524506/1. MCSH acknowledges  
707 support from a Royal Society University Research Fellowship. We would like to thank all the  
708 staff at the Montserrat Volcano Observatory for their assistance during fieldwork. We also  
709 thank Bertrand Leze for analytical assistance. We thank Michael Clynne and Michel  
710 Pichavant for their constructive reviews, which helped to improve this manuscript.

## 711 **References**

- 712 BACHMANN, O. & BERGANTZ, G. W. 2006. Gas percolation in upper-crustal silicic  
713 crystal mushes as a mechanism for upward heat advection and rejuvenation of near-  
714 solidus magma bodies. *Journal of Volcanology and Geothermal Research* **149**, 85-102.
- 715 BACON, C. R. 1986. Magmatic Inclusions in Silicic and Intermediate Volcanic Rocks.  
716 *J. Geophys. Res.* **91**.
- 717 BAN, M., TAKAHASHI, K., HORIE, T. & TOYA, N. 2005. Petrogenesis of Mafic  
718 Inclusions in Rhyolitic Lavas from Narugo Volcano, Northeastern Japan. *Journal of*  
719 *Petrology* **46**, 1543-1563.
- 720 BARCLAY, J., RUTHERFORD, M.J., CARROLL, M.R., MURPHY, M.D., DEVINE, J.D.,  
721 GARDNER, J. & SPARKS, R.S.J. 1998. Experimental phase equilibria constraints on pre-  
722 eruptive storage conditions of the Soufrière Hills magma. *Geophysical Research Letters*  
723 **25**, 3437-3440
- 724 BARCLAY, J., HERD, R. A., EDWARDS, B. R., CHRISTOPHER, T., KIDDLE, E. J., PLAIL,  
725 M. & DONOVAN, A. 2010. Caught in the act: Implications for the increasing abundance of  
726 mafic enclaves during the recent eruptive episodes of the Soufrière Hills Volcano,  
727 Montserrat. *Geophys. Res. Lett.* **37**, L00E09. doi:10.1029/2010GL042509.

728           BLAKE, S. & FINK, J. H. 2000. On the deformation and freezing of enclaves during  
729 magma mixing. *Journal of Volcanology and Geothermal Research* **95**, 1-8.

730           BLAKE, S. & IVEY, G. N. 1986. Magma-mixing and the dynamics of withdrawal from  
731 stratified reservoirs. *Journal of Volcanology and Geothermal Research* **27**, 153-178.

732           BROWNE, B. L., EICHELBERGER, J. C., PATINO, L. C., VOGEL, T. A., DEHN, J., UTO, K.  
733 & HOSHIZUMI, H. 2006a. Generation of Porphyritic and Equigranular Mafic Enclaves  
734 During Magma Recharge Events at Unzen Volcano, Japan. *Journal of Petrology* **47**, 301-  
735 328.

736           BROWNE, B. L., EICHELBERGER, J. C., PATINO, L. C., VOGEL, T. A., UTO, K. &  
737 HOSHIZUMI, H. 2006b. Magma mingling as indicated by texture and Sr / Ba ratios of  
738 plagioclase phenocrysts from Unzen volcano, SW Japan. *Journal of Volcanology and*  
739 *Geothermal Research* **154**, 103-116.

740           BROWNE, B. L. & GARDNER, J. E. 2006. The influence of magma ascent path on the  
741 texture, mineralogy, and formation of hornblende reaction rims. *Earth and Planetary*  
742 *Science Letters* **246**, 161-176.

743           BUCKLEY, V. J. E., SPARKS, R. S. J. & WOOD, B. J. 2006. Hornblende dehydration  
744 reactions during magma ascent at Soufrière Hills Volcano, Montserrat. *Contributions to*  
745 *Mineral Petrology*. **151**, 121-140. DOI 10.1007/s00410-005-0060-5

746           CARDOSO, S. S. S. & WOODS, A. W. 1999. On convection in a volatile-saturated  
747 magma. *Earth and Planetary Science Letters* **168**, 301-310.

748           CLYNNE, M. A. 1989. The disaggregation of quenched magmatic inclusions  
749 contributes to chemical diversity in silicic lavas of Lassen Peak, California. Bull New  
750 Mexico Bureau of Mines and Mineral resources, vol. **131**, p. 54

751           CLYNNE, M. A. 1999. A Complex Magma Mixing Origin for Rocks Erupted in 1915,  
752 Lassen Peak, California. *J. Petrology* **40**, 105-132.

753           COLLINS, W. J., RICHARDS, S. R., HEALY, B. E. & ELLISON, P. I. 2000. Origin of  
754 heterogeneous mafic enclaves by two-stage hybridisation in magma conduits (dykes)  
755 below and in granitic magma chambers. *Geological Society of America Special Papers*  
756 **350**, 27-45.

757           COLLINS, W. J., WIEBE, R. A., HEALY, B. & RICHARDS, S. W. 2006. Replenishment,  
758 Crystal Accumulation and Floor Aggradation in the Megacrystic Kameruka Suite,  
759 Australia. *Journal of Petrology* **47**, 2073-2104.

760 COOMBS, M. L., EICHELBERGER, J. C. & RUTHERFORD, M. J. 2000. Magma storage and  
761 mixing conditions for the 1953-1974 eruptions of Southwest Trident volcano, Katmai  
762 National Park, Alaska. *Contributions to Mineralogy and Petrology* **140**, 99-118.

763 COOMBS, M. L., EICHELBERGER, J. C. & RUTHERFORD, M. J. 2002. Experimental  
764 constraints on mafic enclave formation in volcanic rocks. *Journal of Volcanology and*  
765 *Geothermal Research* **119**, 125-144

766 COUCH, S., SPARKS, R. S. J. & CARROLL, M. R. 2001. Mineral disequilibrium in lavas  
767 explained by convective self-mixing in open magma chambers. *Nature* **411**, 1037-1039.

768 COUCH, S., HARFORD, C.L., SPARKS, R. S. J. & CARROLL, M. 2003b. Experimental  
769 constraints on the conditions of highly calcic plagioclase microlites at the Soufrière Hills  
770 Volcano, Montserrat. *Journal of Petrology* **44**, 1455-1475

771 DEVINE, J. D., MURPHY, M. D., RUTHERFORD, M. J., BARCLAY, J., SPARKS, R. S. J.,  
772 CARROLL, M. R., YOUNG, S. R. & GARDNER, J. E. 1998. Petrologic Evidence for Pre-  
773 Eruptive Pressure-Temperature Conditions, and Recent Reheating, of Andesitic Magma  
774 Erupting at the Soufrière Hills Volcano, Montserrat, W.I. *Geophys. Res. Lett.* **25**.

775 EDMONDS, M., PYLE, D., OPPENHEIMER, C. 2001. A model for degassing at the  
776 Soufrière Hills Volcano, Montserrat, West Indies, based on geochemical evidence. *Earth*  
777 *and Planetary Science Letters* **186**, 159-173.

778 EDMONDS, M., AIUPPA, A., HUMPHREYS, M., MORETTI, R., GIUDICE, G., MARTIN, R.  
779 S., HERD, R. A. & CHRISTOPHER, T. 2010. Excess volatiles supplied by mingling of mafic  
780 magma at an andesite arc volcano. *Geochem. Geophys. Geosyst.* **11**, Q04005.  
781 doi:10.1029/2009GC002781.

782 EDMONDS, M., HUMPHREYS, M. C. S., HAURI, E., HERD, R., WADGE, G., RAWSON, H.,  
783 LEDDEN, R., PLAIL, M., BARCLAY, J., AIUPPA, A., CHRISTOPHER, T., GIUDICE, G. & GUIDA,  
784 R. (this volume). Pre-eruptive vapour and its role in controlling eruption style and  
785 longevity at Soufrière Hills Volcano. *Geol Soc Memoir*.

786 EICHELBERGER, J. C. 1980. Vesiculation of mafic magma during replenishment of  
787 silicic magma reservoirs. *Nature* **288**, 446-450.

788 ELSWORTH, D., MATTIOLI, G., TARON, J., VOIGHT, B. & HERD, R. 2008. Implications  
789 of Magma Transfer Between Multiple Reservoirs on Eruption Cycling. *Science* **322**, 246-  
790 248.

791 FEELEY, T. C., WILSON, L. F. & UNDERWOOD, S. J. 2008. Distribution and  
792 compositions of magmatic inclusions in the Mount Helen dome, Lassen Volcanic Center,  
793 California: Insights into magma chamber processes. *Lithos* **106**, 173-189.

794 FREY, H. M. & LANGE, R. A. 2011. Phenocryst complexity in andesites and dacites  
795 from the Tequila volcanic field, Mexico: Resolving the effects of degassing vs. magma  
796 mixing. *Contributions to Mineralogy and Petrology* **162**, 415-445.

797 GARCIA, M. O. & JACOBSON, S. S. 1979. Crystal clots, amphibole fractionation and the  
798 evolution of calc-alkaline magmas. *Contributions to Mineralogy and Petrology* **69**, 319-  
799 327.

800 GIACHETTI, T., DRUITT, T. H., BURGISSER, A., ARBARET, L. & GALVEN, C. 2010.  
801 Bubble nucleation, growth and coalescence during the 1997 Vulcanian explosions of  
802 Soufrière Hills Volcano, Montserrat. *Journal of Volcanology and Geothermal Research*  
803 **193**, 215-231.

804 GIORDANO, D., RUSSELL, J.K. & DINGWELL, D.B. 2008 Viscosity of magmatic liquids:  
805 A model. *Earth and Planetary Science Letters* **271**, 123-134

806 HARFORD, C. L., PRINGLE, M. S., SPARKS, R. S. J. & YOUNG, S. R. 2002. The volcanic  
807 evolution of Montserrat using 40Ar/39Ar geochronology. *In: Drutt, T.H. & Kokelaar,*  
808 *B.P. (eds). The eruption of the Soufrière Hills Volcano, Montserrat from 1995 to 1999.*  
809 *Geological Society, London, Memoir* **21**, pp. 93-113.

810 HUMPHREYS, M., CHRISTOPHER, T. & HARDS, V. 2009a. Microlite transfer by  
811 disaggregation of mafic inclusions following magma mixing at Soufrière Hills volcano,  
812 Montserrat. *Contributions to Mineralogy and Petrology* **157**, 609-624. Doi:  
813 10.1007/s00410-008-0356-3.

814 HUMPHREYS, M. C. S., EDMONDS, M., CHRISTOPHER, T. & HARDS, V. 2010. Magma  
815 hybridisation and diffusive exchange recorded in heterogeneous glasses from Soufrière  
816 Hills Volcano, Montserrat. *Geophys. Res. Lett.* **37**, L00E06. doi:10.1029/2009GL041926.

817 HUMPHREYS, M.C.S., EDMONDS, M., PLAIL, M., BARCLAY, J., PARKES, D.,  
818 CHRISTOPHER, T. 2012. A new method to quantify the real supply of mafic components to  
819 a hybrid andesite. *Contributions to Mineralogy and Petrology*. In press. DOI:  
820 10.1007/s00410-012-0805-x.

821 LEAKE, B. A., WOOLLEY, A. R., ARPS, C. E. S., BIRCH, W. D., GILBERT, M. C., GRICE,  
822 J. D., HAWTHORNE, F. C., KATO, A., KISCH, H. J., KRIVOVICHEV, V. G., LINTHOUT, K.,  
823 LAIRD, J., MANDARINO, J. A., MARESCH, W. V., NICKEL, E. H., ROCK, N. M. S.,  
824 SCHUMACHER, J. C., SMITH, D. C., C.N, S. N., UNGARETTI, L., WHITTAKER, E. J. W. &  
825 YOUHZI, G. 1997. Nomenclature of Amphiboles: Report of the Subcommittee on  
826 Amphiboles of the International Mineralogical Association, commission on new minerals  
827 and mineral names. *The Canadian Mineralogist* **35**, 219-246.

828 MANN, C.K. 2010. Magma chamber dynamics at Soufrière Hills Volcano, Montserrat.  
829 PhD thesis, McGill University

830 MARTIN, V. M., HOLNESS, M. B. & PYLE, D. M. 2006a. Textural analysis of magmatic  
831 enclaves from the Kameni Islands, Santorini, Greece. *Journal of Volcanology and*  
832 *Geothermal Research* **154**, 89-102.

833 MARTIN, V. M., PYLE, D. M. & HOLNESS, M. B. 2006b. The role of crystal frameworks  
834 in the preservation of enclaves during magma mixing. *Earth and Planetary Science*  
835 *Letters* **248**, 787-799.

836 MATTIOLI, G. S. & HERD, R. 2003. Correlation of cyclic surface deformation recorded  
837 by GPS geodesy with surface magma flux at Soufrière Hills Volcano, Montserrat.  
838 *Seismol. Res. Lett* **74**, 230.

839 MURPHY, M. D., SPARKS, R. S. J., BARCLAY, J., CARROLL, M. R. & BREWER, T. S.  
840 2000. Remobilization of Andesite Magma by Intrusion of Mafic Magma at the Soufrière  
841 Hills Volcano, Montserrat, West Indies. *Journal of Petrology* **41**, 21 - 42.

842 MURPHY, M. D., SPARKS, R. S. J., BARCLAY, J., CARROLL, M. R., LEJEUNE, A. M.,  
843 BREWER, T. S., MACDONALD, R., BLACK, S. & YOUNG, S. 1998. The Role of Magma  
844 Mixing in Triggering the Current Eruption at the Soufrière Hills Volcano, Montserrat,  
845 West Indies. *Geophys. Res. Lett.* **25**.

846 NAKAGAWA, M., WADA, K. & WOOD, C. P. 2002. Mixed Magmas, Mush Chambers  
847 and Eruption Triggers: Evidence from Zoned Clinopyroxene Phenocrysts in Andesitic  
848 Scoria from the 1995 Eruptions of Ruapehu Volcano, New Zealand. *Journal of Petrology*  
849 **43**, 2279-2303.

850 NELSON, S. T. & MONTANA, A. 1992. Sieve-textured plagioclase in volcanic rocks  
851 produced by rapid decompression. *American Mineralogist* **77**, 1242-1249.

852 PALLISTER, J. S., HOBLITT, R. P. & REYES, A. G. 1992. A basalt trigger for the 1991  
853 eruptions of Pinatubo volcano? *Nature* **356**, 426-428.

854 PLECHOV, P.Y., TSAI, A.E., SHCHERBAKOV, D., DIRKSEN, O.V. 2008. Opacitization  
855 conditions of hornblende in Bezymyannyi Volcano andesites (March 30 1956 eruption)  
856 *Petrology* **16**, 19-35

857 RIDOLFI, F. & RENZULLI, A. 2011. Calcic amphiboles in calc-alkaline and alkaline  
858 magmas: thermobarometric and chemometric empirical equations valid up to 1,130\_C  
859 and 2.2 GPa. *Contributions to Mineralogy and Petrology* **163**, 877-895.

860 RUPRECHT, P. & WÖRNER, G. 2007. Variable regimes in magma systems documented  
861 in plagioclase zoning patterns: El Misti stratovolcano and Andahua monogenetic cones.  
862 *Journal of Volcanology and Geothermal Research* **165**, 142-162.

863 RUTHERFORD, M. J. & DEVINE, J. D. 2003. Magmatic Conditions and Magma Ascent  
864 as Indicated by Hornblende Phase Equilibria and Reactions in the 1995-2002 Soufrière  
865 Hills Magma. *J. Petrology* **44**, 1433-1453.

866 SINGER, B. S., DUNGAN, M. A. & LAYNE, G. D. 1995. Textures and Sr, Ba, Mg, Fe, K  
867 and Ti compositional profiles in volcanic plagioclase clues to the dynamics of calc-  
868 alkaline magma chambers. *American Mineralogist* **80**, 776-798.

869 SNYDER, D., CRAMBES, C., TAIT, S. & WIEBE, R. A. 1997. Magma Mingling in Dikes  
870 and Sills. *The Journal of Geology* **105**, 75-86.

871 SPARKS, R. S. J. & MARSHALL, L. A. 1986. Thermal and mechanical constraints on  
872 mixing between mafic and silicic magmas. *Journal of Volcanology and Geothermal  
873 Research* **29**, 99-124.

874 SPARKS, R.S.J., MURPHY, M.D., LEJEUNE, A.M., WATTS, R.B., BARCLAY, J. & YOUNG,  
875 S.R. 2000. Control on the emplacement of the andesite lava dome of the Soufrière Hills  
876 volcano, Montserrat by degassing-induced crystallization. *Terra Nova* **12**, 14-20.

877 STINTON, A.J., COLE, P.D., ODBERT, H.M., *et al.* (this volume) Geomorphic changes at  
878 the Soufrière Hills Volcano, Montserrat, during a short intensive episode of dome growth:  
879 4 October 2009 - 11 February 2010. *Geol. soc memoir*

880 TEPLY, F. J., DAVIDSON, J. P. & CLYNNE, M. A. 1999. Magmatic Interactions as  
881 Recorded in Plagioclase Phenocrysts of Chaos Crags, Lassen Volcanic Center, California.  
882 *Journal of Petrology* **40**, 787-806.

883 THOMAS, N. & TAIT, S. R. 1997. The dimensions of magmatic inclusions as a  
884 constraint on the physical mechanism of mixing. *Journal of Volcanology and Geothermal  
885 Research* **75**, 167-178.

886 TURNBULL, R., WEAVER, S., TULLOCH, A., COLE, J., HANDLER, M. & IRELAND, T.  
887 2010. Field and Geochemical Constraints on Mafic–Felsic Interactions, and Processes in  
888 High-level Arc Magma Chambers: an Example from the Halfmoon Pluton, New Zealand.  
889 *Journal of Petrology* **51**, 1477-1505.

890 WADGE, G., VOIGHT, B., SPARKS, R.S.J., COLE, P., LOUGHLIN, S.C. (this volume) An  
891 overview of the Soufrière Hills Volcano from 2000 -2010. *Geol. soc. memoir*



892 WIEBE, R. A. 1993. The Pleasant Bay Layered Gabbro—Diorite, Coastal Maine:  
893 Ponding and Crystallization of Basaltic Injections into a Silicic Magma Chamber. *Journal*  
894 *of Petrology* **34**, 461-489.

895 WIEBE, R. A., SMITH, D., STURM, M., KING, E. M. & SECKLER, M. S. 1997. Enclaves in  
896 the Cadillac Mountain Granite (Coastal Maine): Samples of Hybrid Magma from the  
897 Base of the Chamber. *Journal of Petrology* **38**, 393-423.

898 ZELLMER, G. F. HAWKESWORTH., C. J. SPARKS, R. S. J. THOMAS, L. E. HARFORD, C. L.  
899 BREWER, T. S. LOUGHLIN, S. C. 2003. Geochemical Evolution of the Soufrière Hills  
900 Volcano, Montserrat, Lesser Antilles Volcanic Arc. *Journal of Petrology* **44**, 1349 -1374.  
901

## 902 **Figures**

903 **Figure 1:** (a) A representative image of an andesitic block from Feb 11 2010 dome collapse  
904 (scale: 10 cm with 2 cm intervals). (b) is an image of the net employed during point counting  
905 of mafic enclaves. Net is 1m<sup>2</sup>, string is spaced at 10 cm intervals, with 2 cm tick marks. (c)  
906 Image of type A and B enclaves seen in the field. Note distinct colour difference and the  
907 clearly distinct margins in A as opposed to B (d) shows typical diktytaxitic framework  
908 observed in mafic enclaves with inherited phenocrysts of plagioclase (plag), amphibole (amp)  
909 and orthopyroxene (opx).

910 **Figure 2:** Frequency size distribution of measured enclave apparent diameters from andesitic  
911 blocks used to evaluate mafic enclave abundance in Table 2.

912 **Figure 3:** Inherited plagioclase phenocrysts overgrowth rim width (measured distance from  
913 crystal edge to sieve-texture) versus sieve-texture width. Increasing rim width is correlated  
914 with sieve-texture width. Note that where sieve-texture width is greater than 1000µm the  
915 sieve-texture pervades through to the crystal core.

916 **Figure 4:** All images are representative of type A enclaves. (a) Large type A enclave from  
917 Feb 11 2010 dome collapse deposit. Darkening of andesite around the enclave is an artefact  
918 of water spray used to clean the outcrop (scale: 10 cm with 2 cm intervals) (b)  
919 Photomicrograph of a type A chilled margin shown by a reduction in framework crystal size;  
920 andesite is on the left and mafic enclave on the right (c) Photomicrograph of type A  
921 framework crystals, Fe-Ti oxides (ox) (d) BSE image of framework plagioclase with sieve-

922 texture developing in the interior of the crystal. (e) BSE image of a clinopyroxene reaction  
923 rim developing on a high-Al amphibole microphenocryst.

924 **Figure 5:** Vesicle size distribution of measured type A and B enclaves.

925 **Figure 6:** Total inherited phenocryst modal proportions by enclave type against SiO<sub>2</sub>  
926 composition. A total of 16 enclaves were used and we observe that enclave types A and B  
927 plot in two distinct fields. Details of the inherited phenocryst type proportions counting are  
928 shown in Table 4.

929 **Figure 7:** Groundmass glass compositions of enclave types from electron probe analyses. (a)  
930 SiO<sub>2</sub> vs. K<sub>2</sub>O. Type Ci (interior of portion of composite enclave), Type Ce (exterior portion)  
931 (b) FeO\*<sub>tot</sub> vs. MgO.

932 **Figure 8:** (a) to (d) are representative of type B enclaves; (e) to (f) are representative of type  
933 C. (a) Type B enclaves sized from 2 cm to >10 cm in a single andesite block from Feb 11  
934 2010 dome collapse deposit (scale: 10 cm with 2 cm intervals) (b) Photomicrograph of a  
935 diffuse margin between the host andesite and type B enclave. (c) Photomicrograph of small  
936 orthopyroxene microlites growing outwards from vesicle walls in pools of glass.  
937 Concentrations of glass are often associated with larger coalesced vesicles. (d) BSE image of  
938 a type B groundmass. Note zoning of opx crystal to cpx from core to rim. (e) Hand specimen  
939 image of the type C enclave used for this study (MT08) with an inner mafic portion and a  
940 hybrid mafic exterior portion (f) Photomicrograph of the margin between the inner and outer  
941 enclave portions The interior to the right of the margin contains more glass and high-Al  
942 amphibole microphenocrysts than the exterior portion to the left of the margin.

943 **Figure 9:** Comparison of XRF bulk geochemistry of mafic enclaves and host andesite across  
944 the first five phases of extrusive activity. Open symbols are SHV andesite and closed  
945 symbols are mafic enclaves. Phase I (Murphy *et al.* 2000; Zellmer *et al.* 2003); Phase II  
946 (Mann 2010; Zellmer *et al.* 2003); Phase III (Barclay *et al.* 2010; this study); Phases IV to V  
947 (this study)

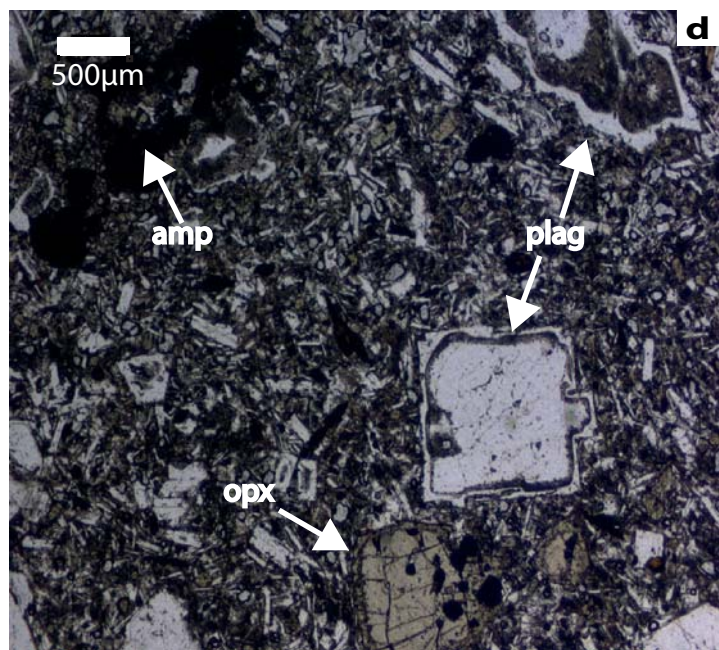
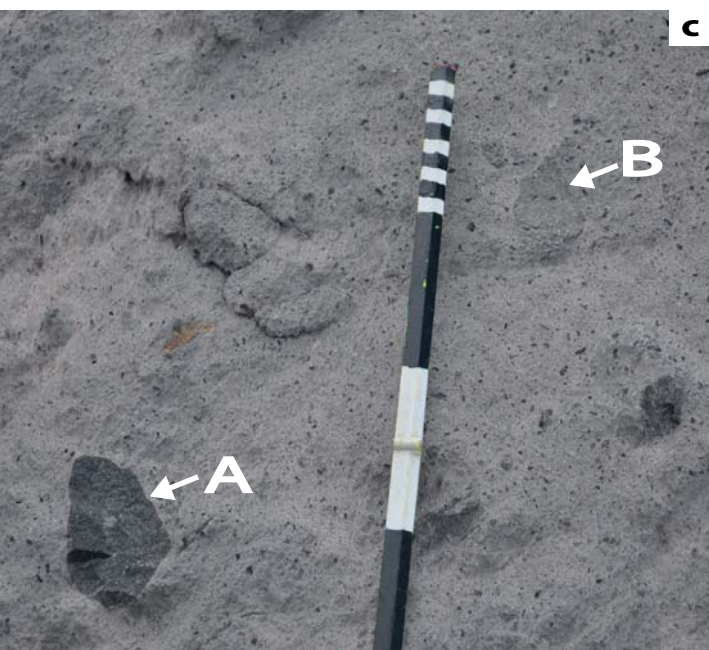
948 **Figure 10:** Comparison of mafic enclave types A, B and C from Phase V using representative  
949 XRF bulk geochemistry data. Arrows indicate projected effect of adding equal proportions of  
950 inherited plagioclase and amphiboles phenocrysts to the least evolved mafic enclave bulk  
951 composition.

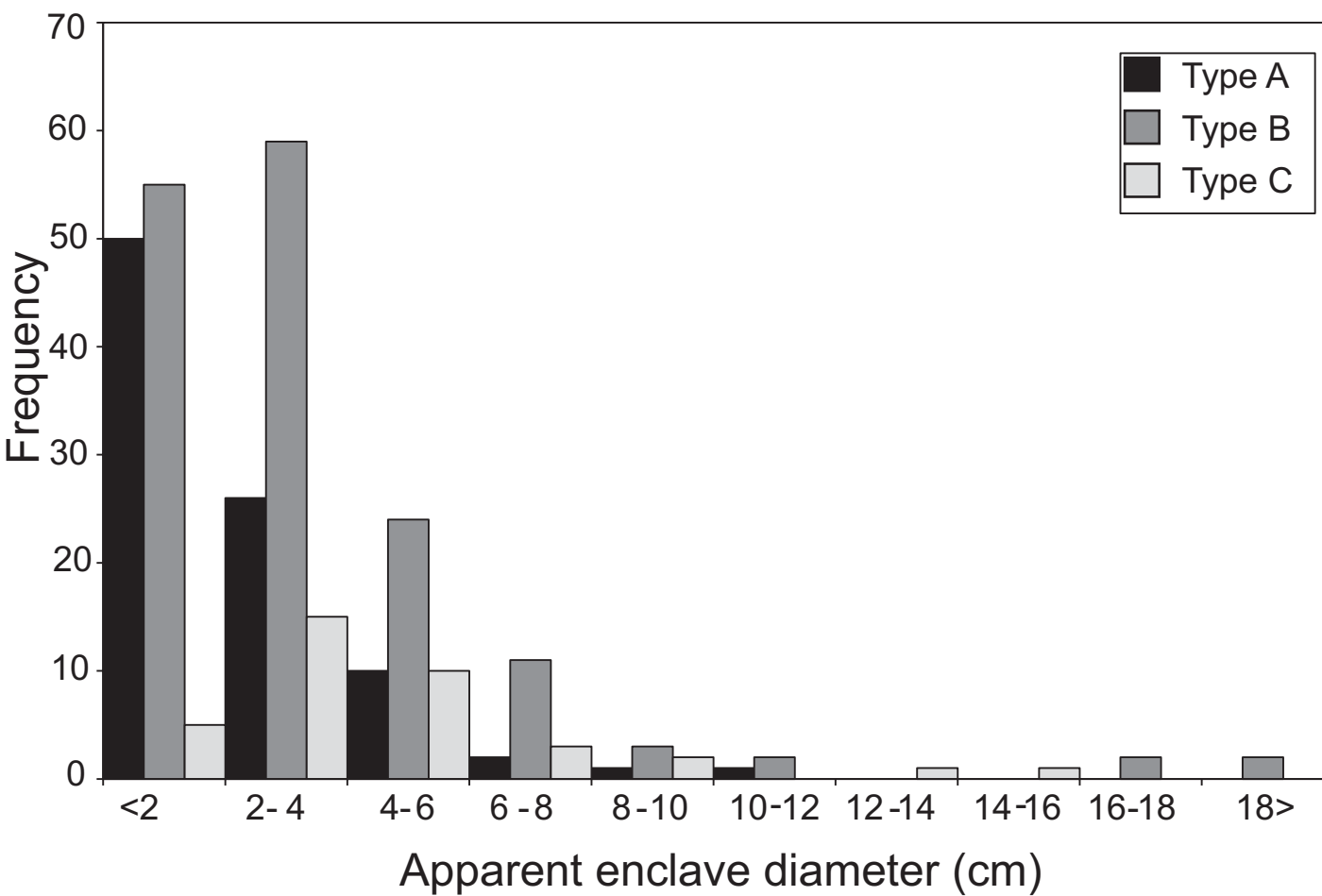
952 **Figure 11:** Simplified modelled effective viscosity of SHV host andesite and mafic enclaves  
953 against temperature. Melt viscosity was modelled using the method of Giordano *et al.* (2008)  
954 and effective viscosity using the Einstein-Roscoe relation. Andesite sample has 77 wt % SiO<sub>2</sub>  
955 40% crystals, 4% wt % H<sub>2</sub>O. We use three enclave samples using measured bulk  
956 compositions, and assume modal inherited phenocryst proportions are mixed in prior to  
957 enclave formation. Type A (MT27) is the least evolved phase V sample with 49 wt % SiO<sub>2</sub>,  
958 8% inherited phenocryst volume, and 6 wt % H<sub>2</sub>O. Type B end-members were modelled (1)  
959 53 wt % SiO<sub>2</sub> and 16% inherited phenocrysts, 6 wt % H<sub>2</sub>O (2) 58 wt % SiO<sub>2</sub>, 24% inherited  
960 phenocrysts, and 6 wt % H<sub>2</sub>O. We assume mafic magma temperatures of between 950-  
961 1100°C, and similar temperatures for Types A and B for the purposes of this model, H<sub>2</sub>O  
962 contents from Edmonds *et al.* (this volume) and andesite temperatures from Barclay *et al.*  
963 (1998).

964 **Figure 12:** Proposed mingling model for Phase V from petrological, textural and  
965 geochemical analysis of mafic enclave types. (A) Type A enclaves form during intrusion of a  
966 mafic magma plume either at plume margins or from ‘spray’. Collapse of plume as indicated  
967 by arrows is driven by both density and gravity contrasts, or by a reduction in the rate of  
968 mafic injection. Andesite derived phenocrysts and melt are engulfed by the intruding mafic  
969 magma forming a hybrid mafic magma, which ponds towards the magma chamber base, with  
970 perhaps denser material at the base. (B) Hybridised mafic magma derived from the collapse  
971 of a plume; hybridised as a result of localised mixing with the andesite is shown at the base of  
972 the chamber. At the hybrid mafic-andesite interface crystallisation results due to cooling of  
973 the hybrid mafic layer. Type B enclaves are derived from this layer either as the result of  
974 blobs of magma detaching from the layer or breakup of the layer. Mafic material may also  
975 continue to pond at the base of the chamber beneath the mafic hybrid due to quasi-continuous  
976 input of mafic material. (C) Type C enclaves may be the result of multiple injections of mafic  
977 magma. Blobs of mafic magma may detach from the intruding magma as it intrudes through  
978 the mafic hybrid, mingling with the hybrid magma. Composite enclave textures are only  
979 likely to form where viscosity and temperature contrast is greatest between the mafic and  
980 mafic hybrid *i.e.* close to the mafic-silicic interface.

981

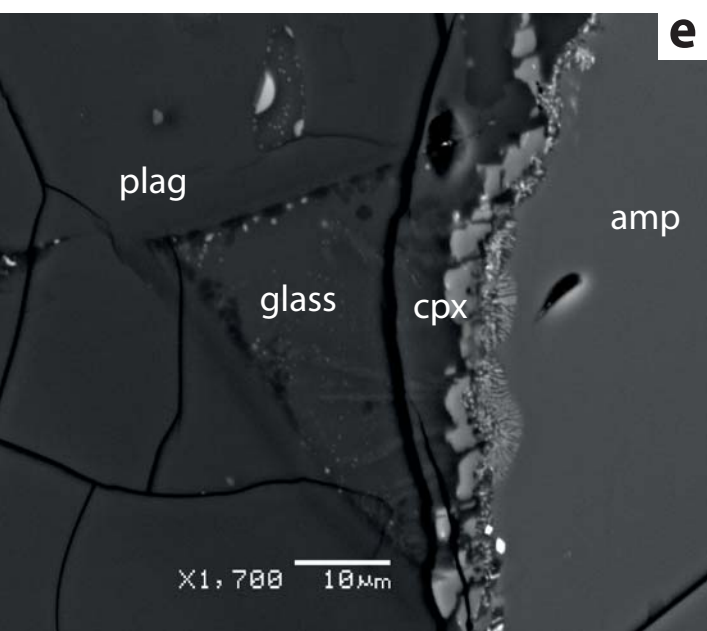
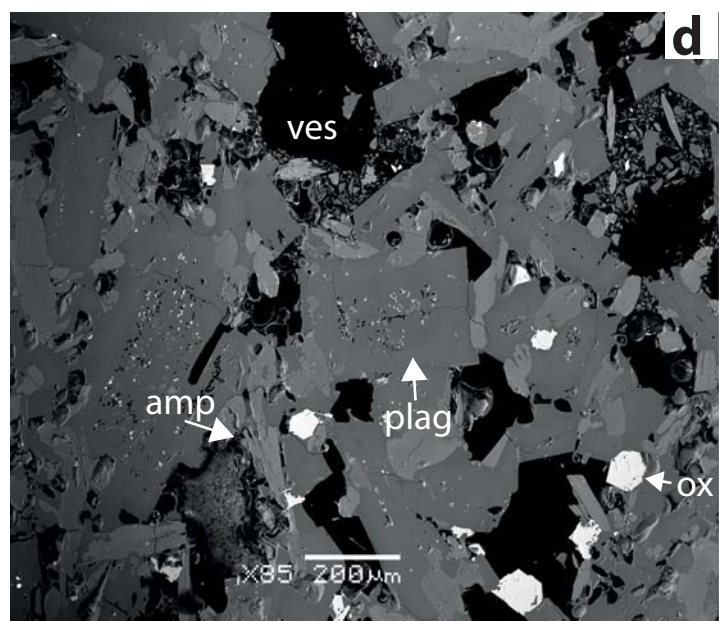
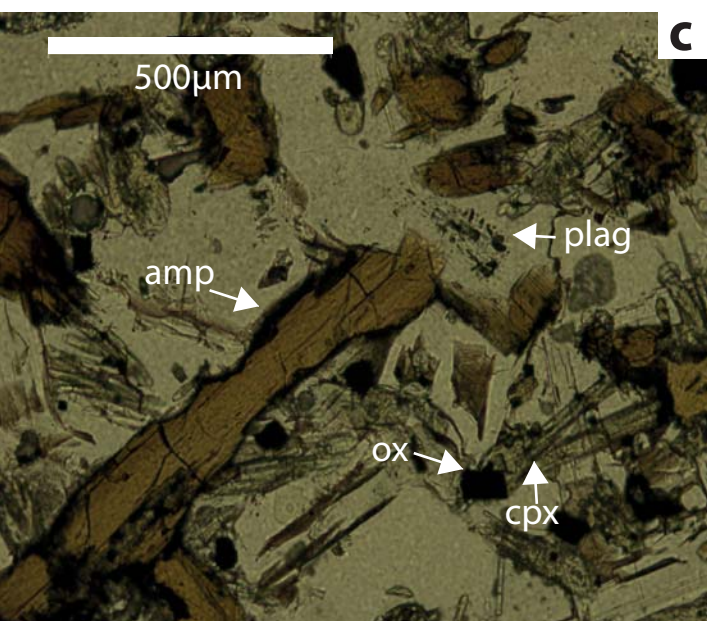
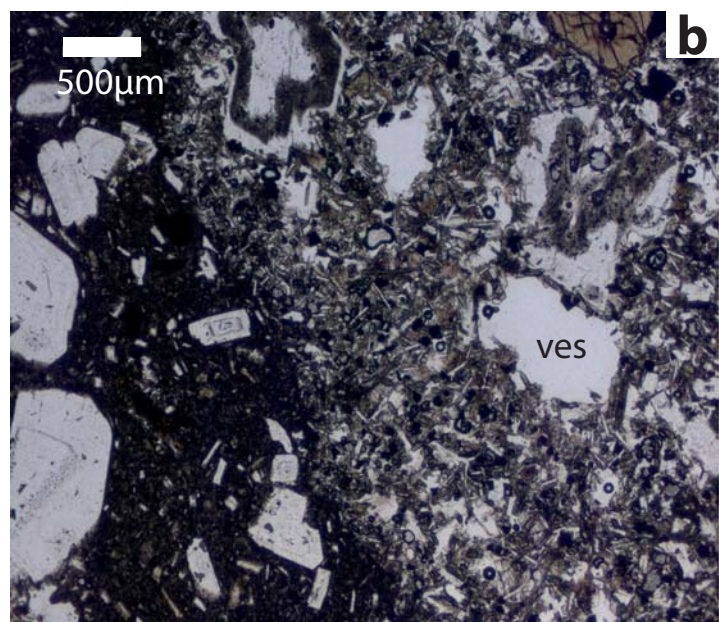
982

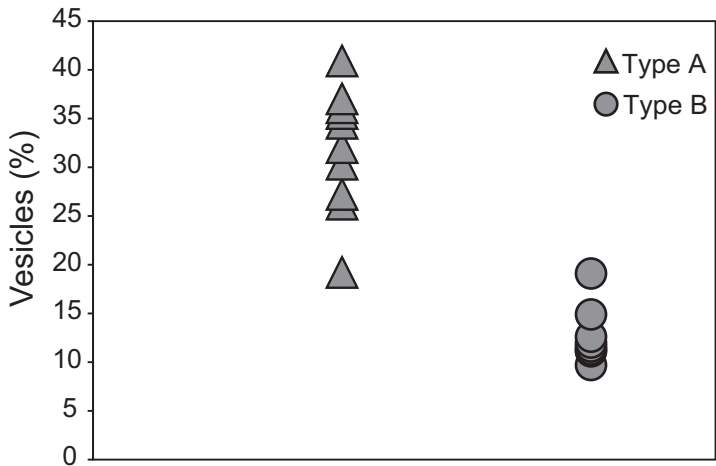




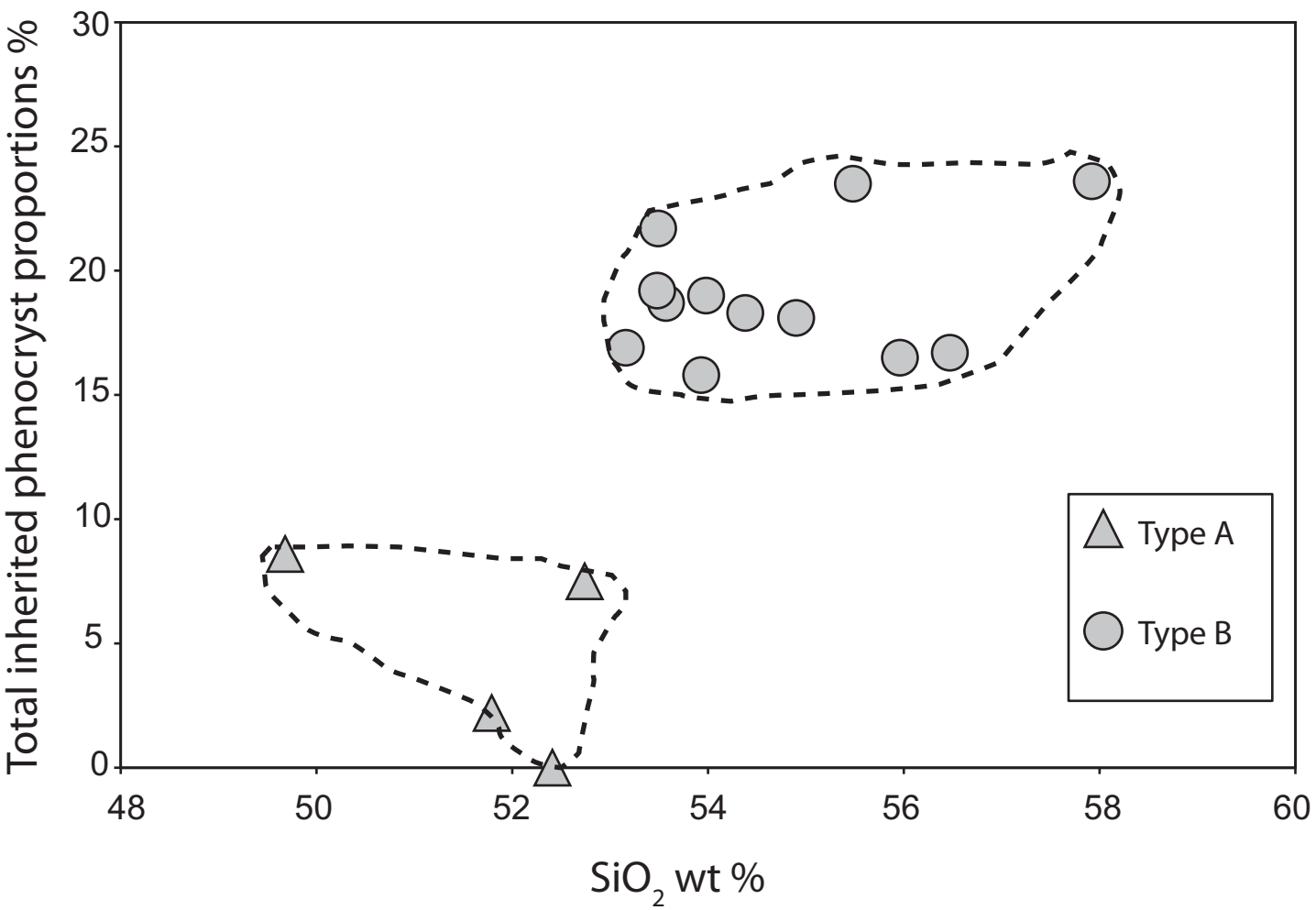


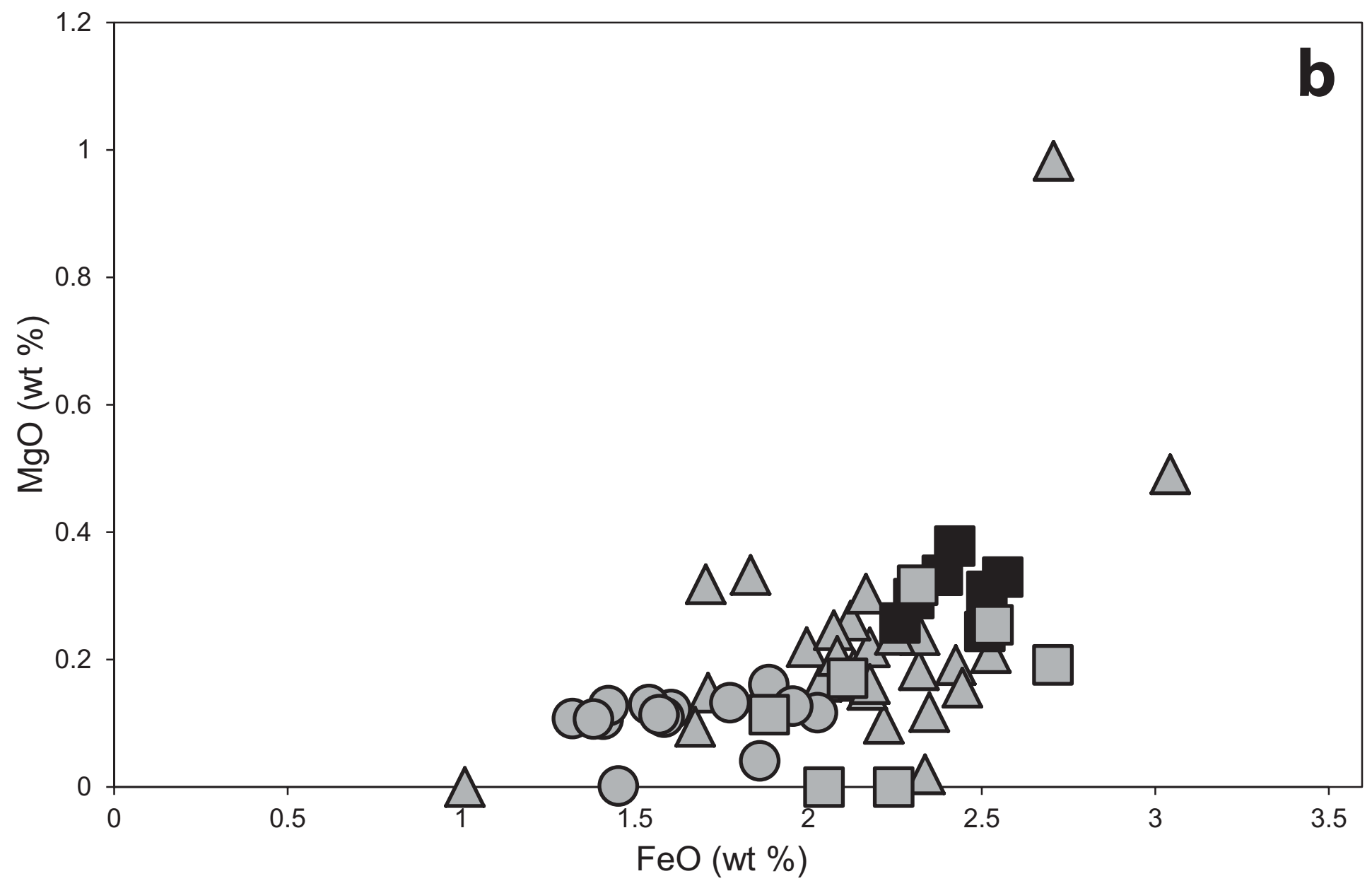
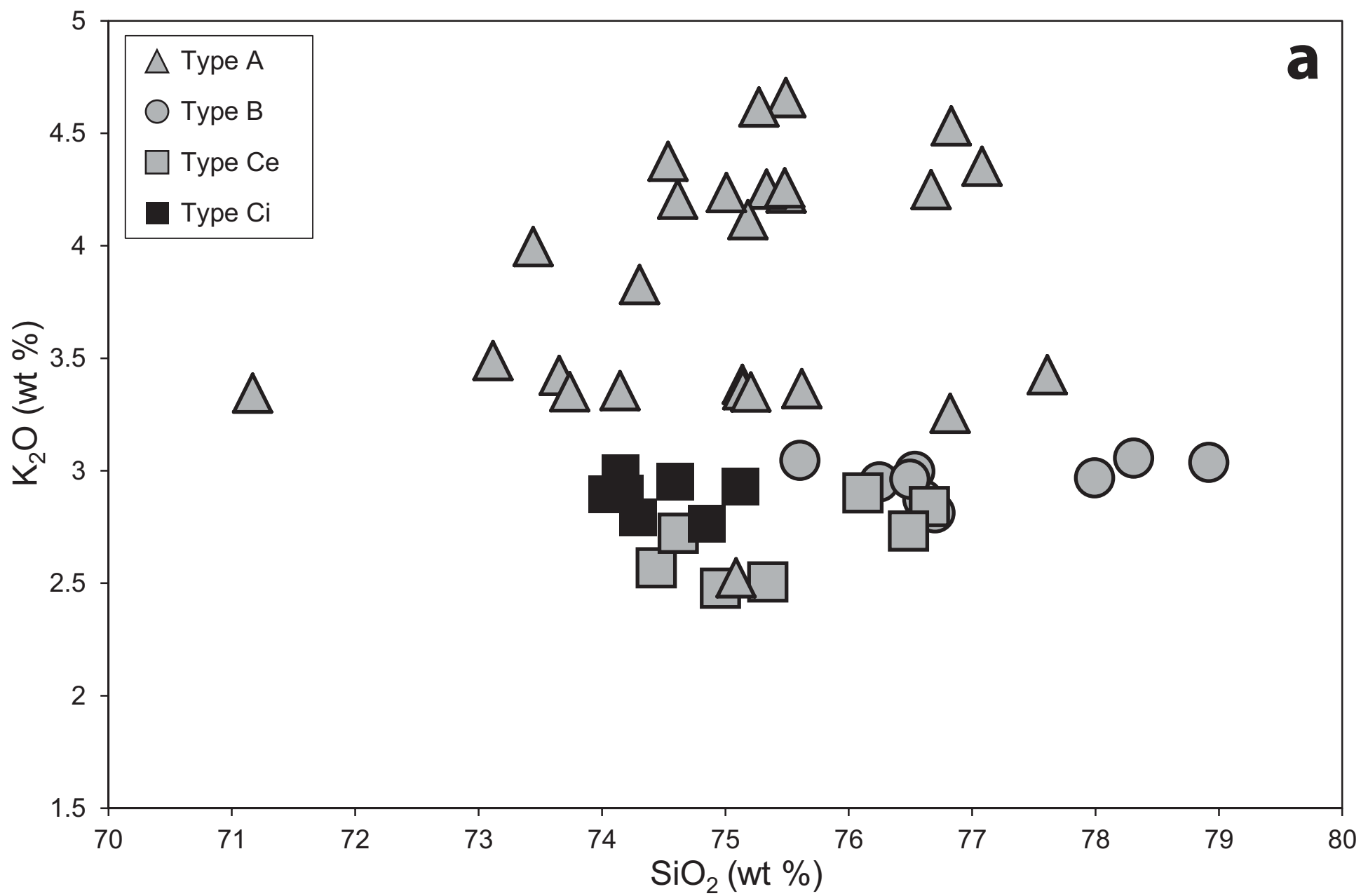




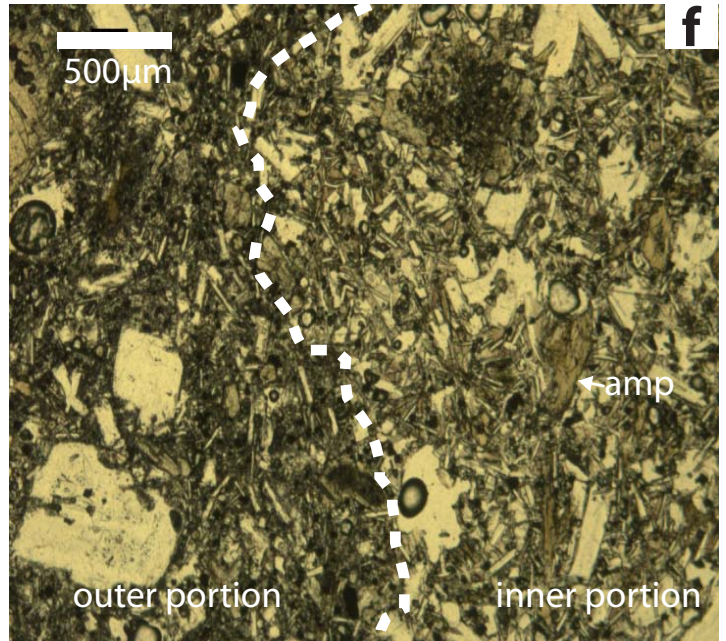
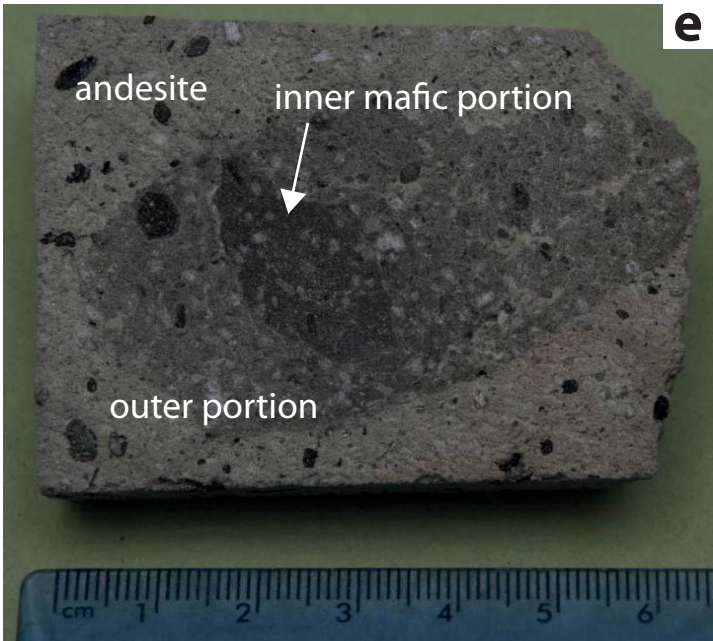
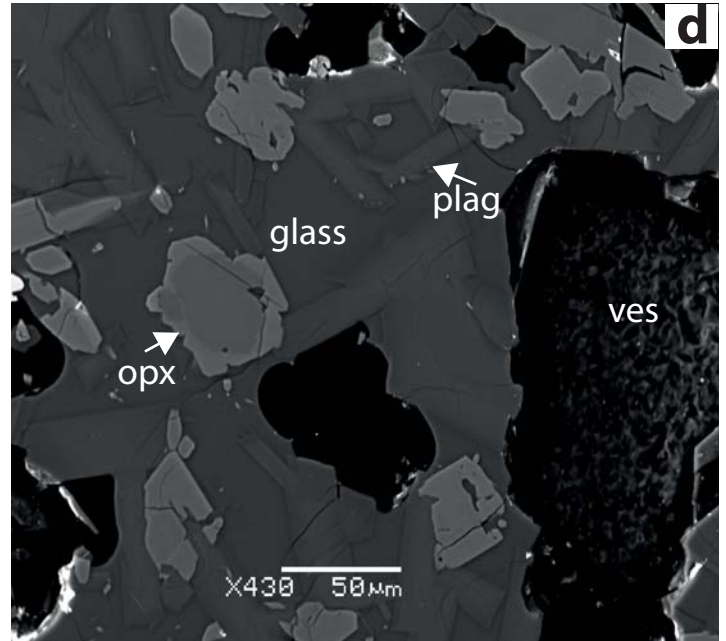
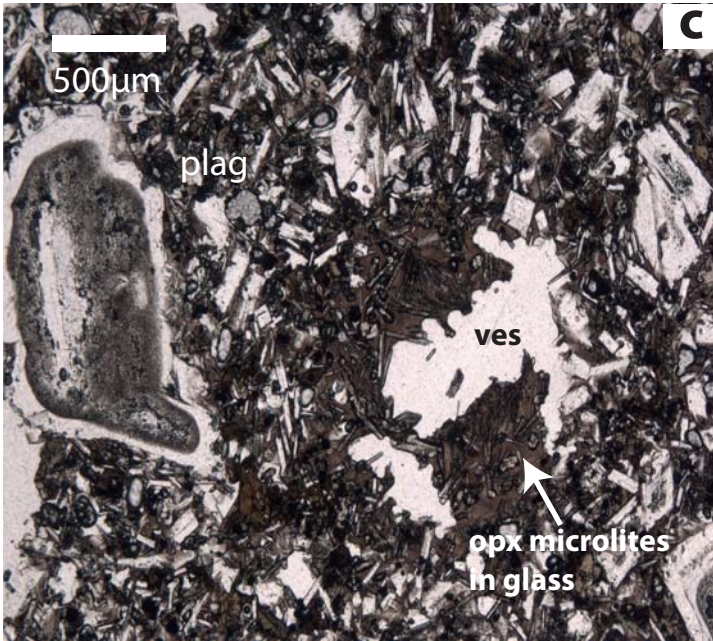
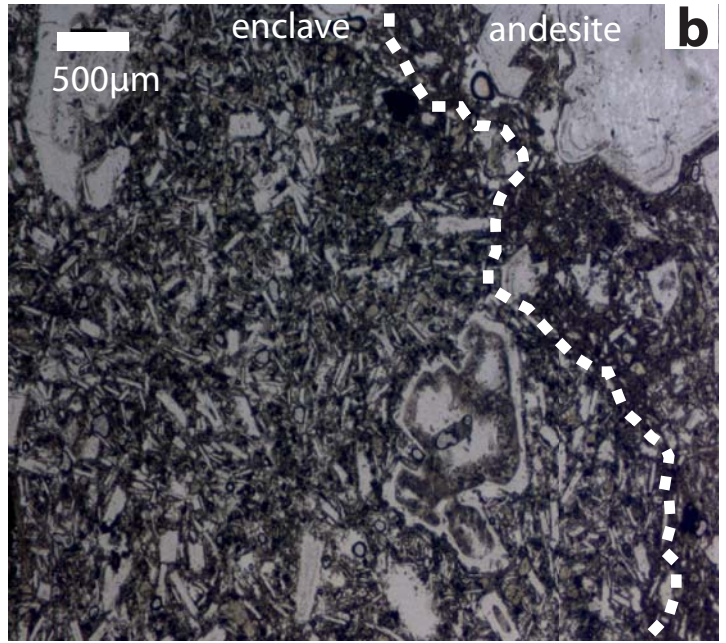




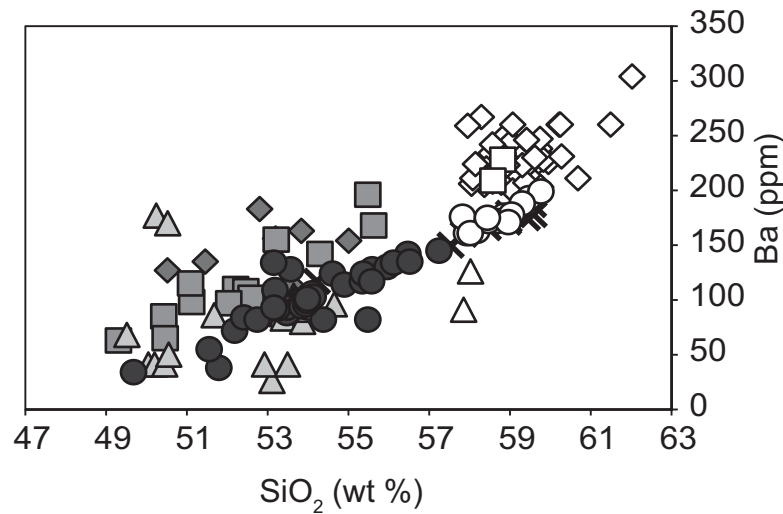
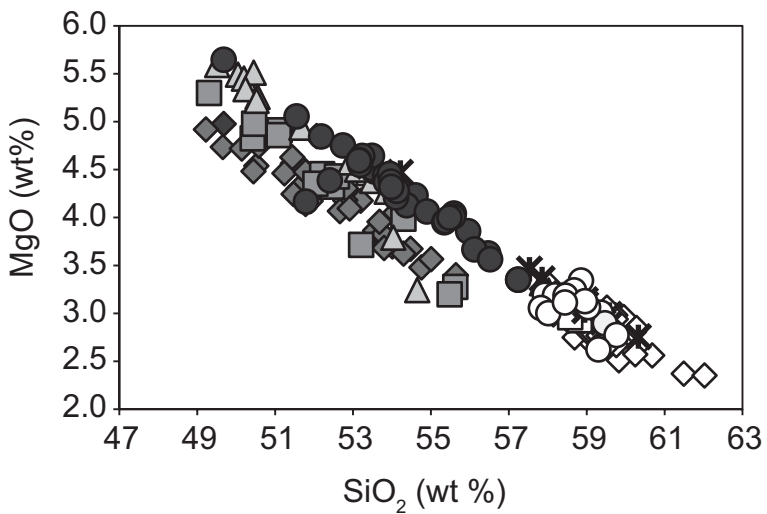
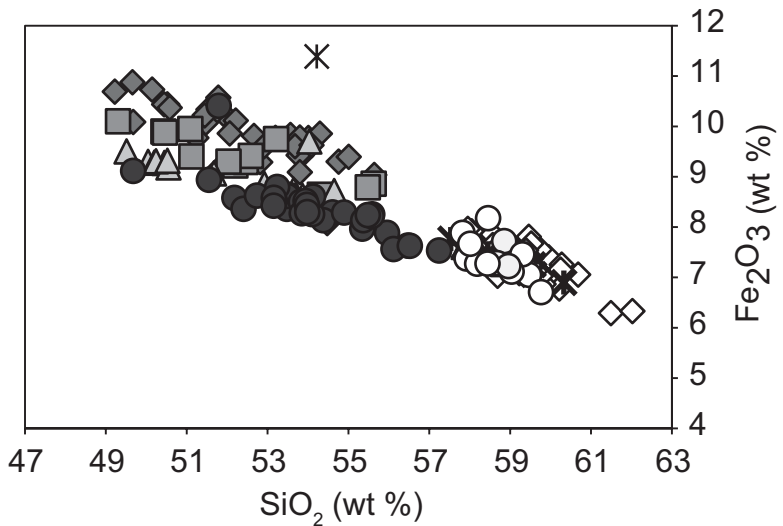
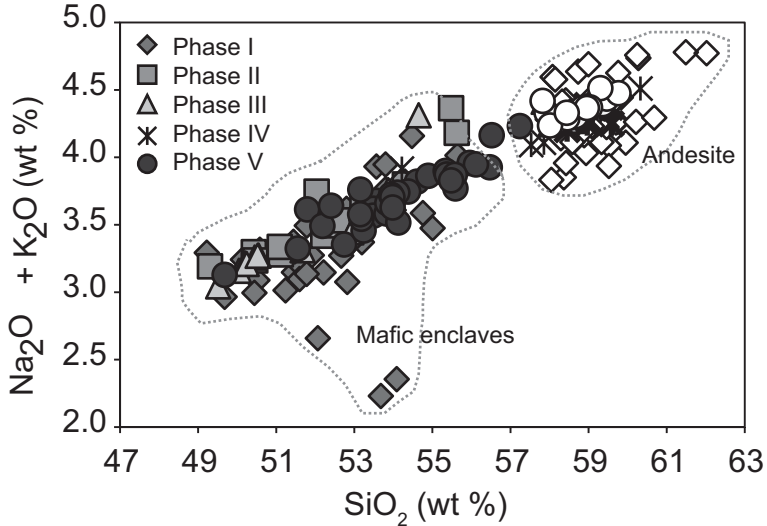


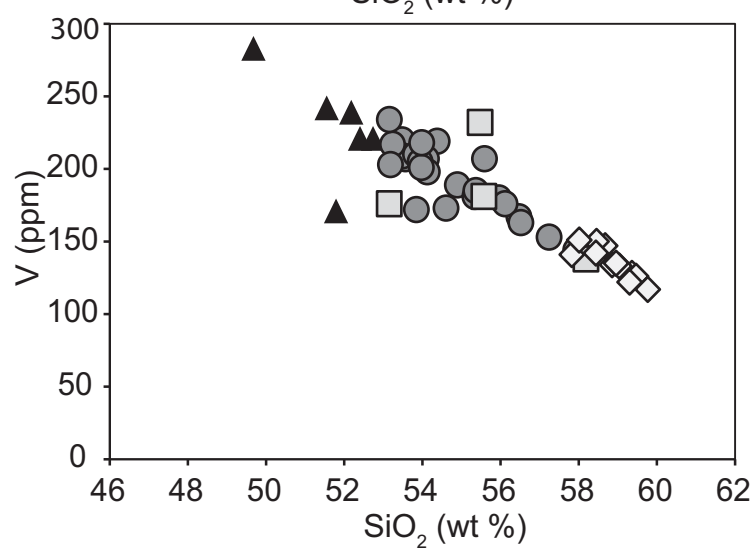
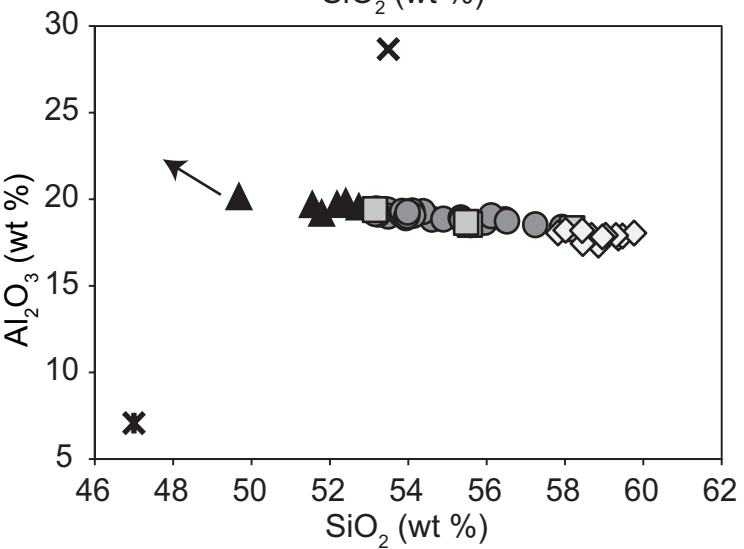
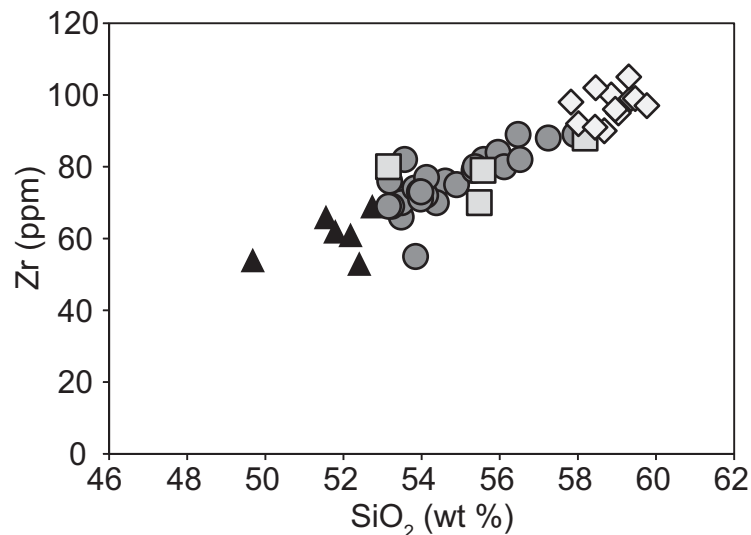
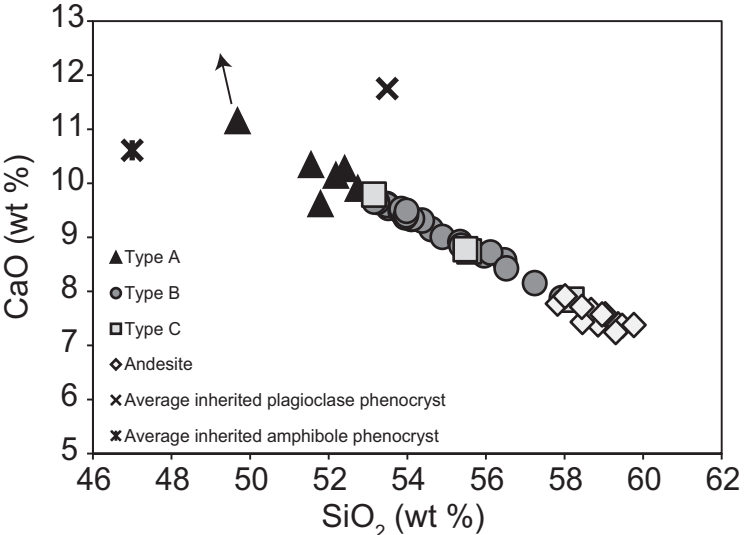


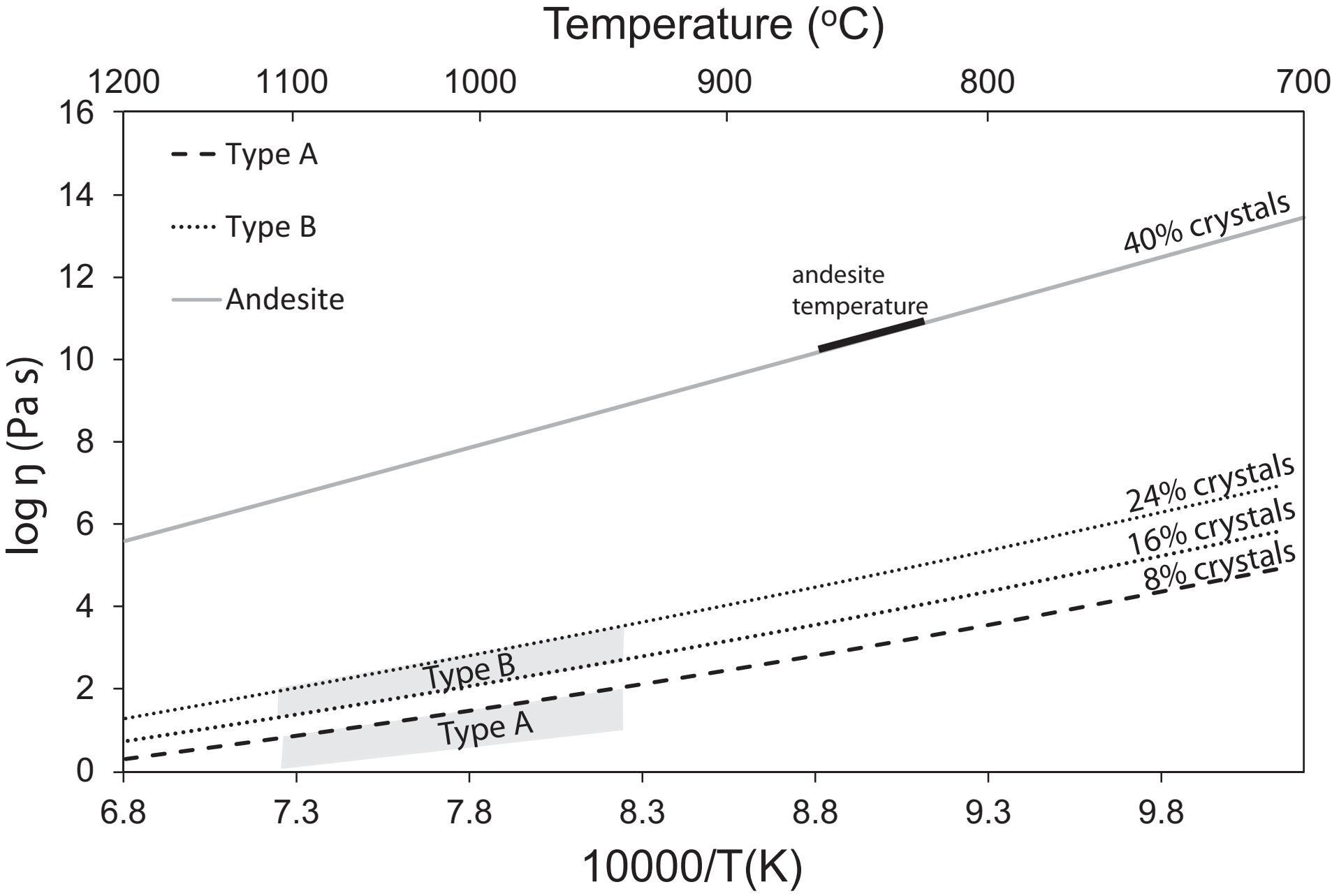


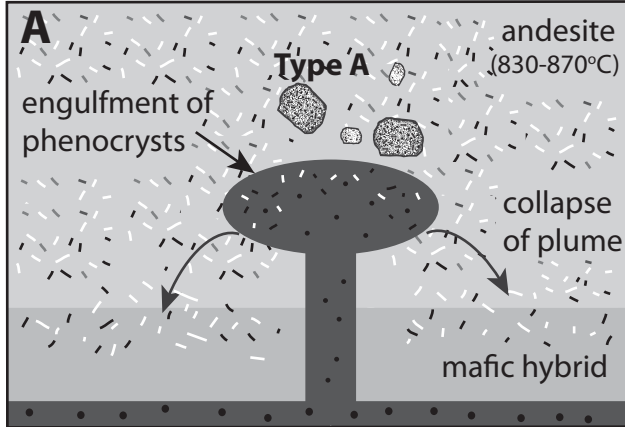












mafic input  
(~1000°C)

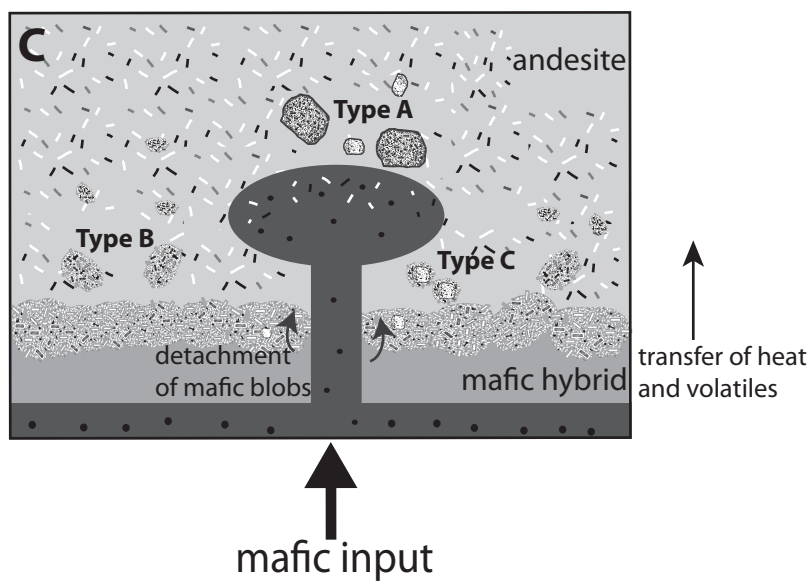
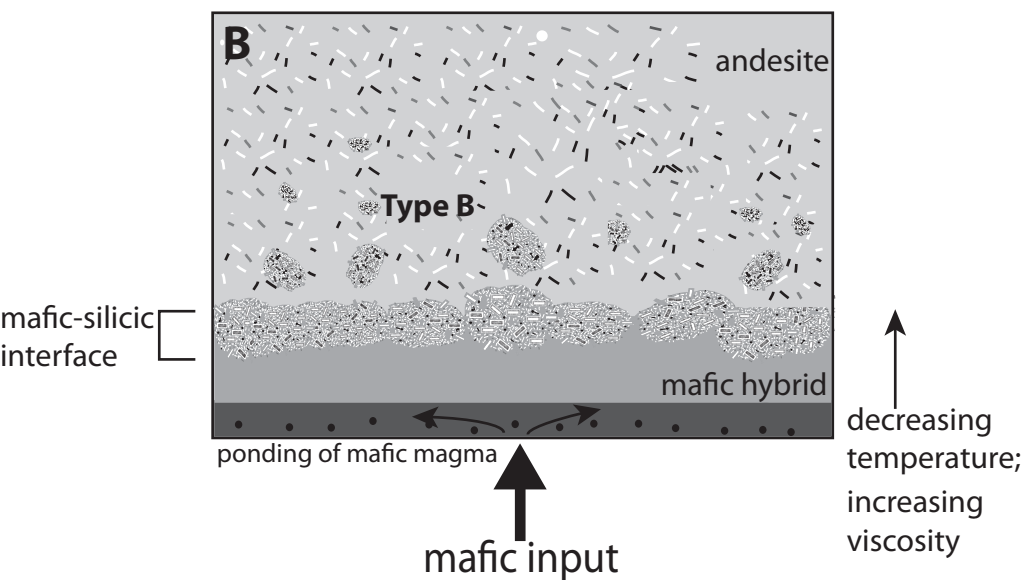


**Table 1:** *Phase IV and V sample locations*

| <b>Sample no.</b>                | <b>Location</b> | <b>GPS</b> |         | <b>Source</b>       | <b>Date of emplacement</b> |
|----------------------------------|-----------------|------------|---------|---------------------|----------------------------|
| MVO1535                          | Lower Gages     |            |         | Vulcanian explosion | 03-Jan-2009                |
| MT18-19, MVO1588, 1590,1591,1593 | Aymers          | 583522     | 1846419 | Pyroclastic flow    | Jan-2010                   |
| MVO1566                          | Whites River    | 586880     | 1845330 | Pyroclastic flow    | Jan-2010                   |
| MVO1567                          | Bugby Hole      | 587400     | 1851433 | Dome collapse       | 11-Feb-2010                |
| MT20-MT37                        | Trants          | 589511     | 1852588 | Dome collapse       | 11-Feb-2010                |
| MT06-MT11                        | Streatham ridge | 586695     | 1850599 | Dome collapse       | 11-Feb-2010                |

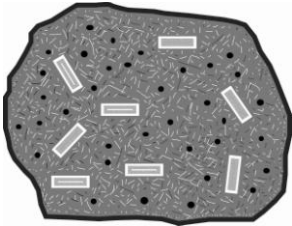
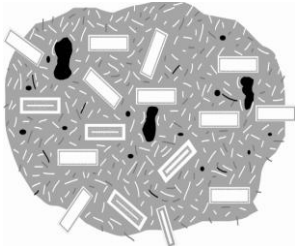


**Table 2.** *Phase V mafic enclave proportional abundances*

| <b>Enclave type</b>               | <b>Block 1a*</b> | <b>Block 1b*</b> | <b>Block 2</b> | <b>Block 3</b> | <b>Block 4</b> | <b>Block 5</b> | <b>Block 6</b> | <b>Block 7</b> |
|-----------------------------------|------------------|------------------|----------------|----------------|----------------|----------------|----------------|----------------|
| Total points                      | 1326             | 2550             | 2397           | 2397           | 2397           | 2397           | 2295           | 2601           |
| Total enclaves points             | 47               | 155              | 137            | 196            | 125            | 115            | 67             | 126            |
| Overall % of magmatic enclaves    | 3.54             | 6.08             | 5.72           | 8.18           | 5.21           | 4.80           | 2.92           | 4.84           |
| Total number of enclaves measured | 20               | 30               | 46             | 39             | 48             | 43             | 30             | 29             |
| <i>Type %</i>                     |                  |                  |                |                |                |                |                |                |
| <i>A</i>                          | 0.00             | 30.32            | 13.14          | 4.59           | 27.20          | 27.83          | 46.27          | 29.37          |
| <i>B</i>                          | 100.00           | 60.65            | 77.37          | 80.61          | 54.40          | 31.30          | 52.24          | 52.38          |
| <i>C</i>                          | 0.00             | 9.03             | 9.49           | 14.80          | 18.40          | 40.87          | 1.49           | 18.25          |

\*Block 1a and 1b is the same block, but two different faces were analysed

**Table 3.** Summary of key features of enclave types A and B

| Type |   | Composition                 | Margin               | Vesicularity   | Framework crystals               | Inherited phenocryst abundance | Inherited plagioclase phenocryst rim thickness |
|------|---|-----------------------------|----------------------|----------------|----------------------------------|--------------------------------|--|
| A    |  | 49-52 wt % SiO <sub>2</sub> | Chilled              | 32% vol (mean) | High-Al amphibole present        | <8% vol                        | 132-230μm                                      |
| B    |  | 53-57 wt % SiO <sub>2</sub> | Unchilled to diffuse | 13% vol (mean) | High-Al amphibole rare to absent | 15-25% vol                     | 27-113μm                                       |

**Table 4.** *Inherited phenocryst proportional abundances of phase V enclave types*

| <b><i>Inherited Phenocryst Type</i></b> | <b><i>Type A (%)</i></b> | <b><i>Type B (%)</i></b> | <b><i>Type C: inner (%)</i></b> | <b><i>Type C: exterior (%)</i></b> |
|---|--------------------------|--------------------------|---------------------------------|------------------------------------|
| <i>Plagioclase Type 1</i>               | 0                        | 0.5-10.9                 | 0                               | 1.9                                |
| <i>Plagioclase Type 2</i>               | 0 -7                     | 5 - 21                   | 8.9                             | 13                                 |
| Plagioclase Total                       | 0 -7                     | 8 - 21.2                 | 8.9                             | 14.9                               |
| Amphibole                               | 0 - 2.9                  | 1.2 - 8.5                | 3.3                             | 6.7                                |
| Orthopyroxene                           | 0 - 0.6                  | 0.4 - 4.5                | 0                               | 4.5                                |
| <b>Total Range</b>                      | <b>0-8</b>               | <b>15.8 - 23.6</b>       | <b>12.6</b>                     | <b>26.5</b>                        |

**Table 5. Average compositions of selected minerals from mafic enclaves**

| <b>a) Plagioclase framework (core)</b> |               |      |               |      |                        |      |                        |      |
|--|---------------|------|---------------|------|------------------------|------|------------------------|------|
|  | <b>Type A</b> |      | <b>Type B</b> |      | <b>Type C Interior</b> |      | <b>Type C Exterior</b> |      |
|  | $\pm 1\sigma$ |      | $\pm 1\sigma$ |      | $\pm 1\sigma$          |      | $\pm 1\sigma$          |      |
| <i>n</i>                               | 22            |      | 18            |      | 9                      |      | 7                      |      |
| SiO <sub>2</sub>                       | 47.02         | 1.80 | 49.90         | 1.89 | 45.82                  | 0.94 | 48.86                  | 1.15 |
| TiO <sub>2</sub>                       | 0.02          | 0.01 | 0.03          | 0.01 | 0.02                   | 0.01 | 0.03                   | 0.01 |
| Al <sub>2</sub> O <sub>3</sub>         | 33.12         | 1.29 | 31.17         | 1.13 | 32.84                  | 0.79 | 30.62                  | 1.01 |
| FeO                                    | 0.61          | 0.09 | 0.68          | 0.06 | 0.59                   | 0.04 | 0.70                   | 0.06 |
| SrO                                    | 0.03          | 0.03 | 0.04          | 0.01 | 0.01                   | 0.06 | 0.03                   | 0.04 |
| MgO                                    | 0.08          | 0.02 | 0.07          | 0.02 | 0.07                   | 0.03 | 0.08                   | 0.02 |
| CaO                                    | 17.12         | 1.36 | 14.68         | 1.35 | 17.02                  | 0.68 | 14.89                  | 0.94 |
| Na <sub>2</sub> O                      | 1.82          | 0.80 | 3.28          | 0.82 | 1.76                   | 0.39 | 3.01                   | 0.52 |
| K <sub>2</sub> O                       | 0.03          | 0.03 | 0.06          | 0.02 | 0.02                   | 0.02 | 0.06                   | 0.02 |
| Total                                  | 99.82         |      | 99.93         |      | 98.12                  |      | 98.34                  |      |
| X <sub>An</sub>                        | 83.72         | 6.98 | 71.03         | 7.06 | 84.12                  | 3.46 | 72.98                  | 4.66 |

| <b>b) Amphibole (core)</b>     |               |      |               |      |                        |      |                        |  |
|--------------------------------|---------------|------|---------------|------|------------------------|------|------------------------|--|
|                                | <b>Type A</b> |      | <b>Type B</b> |      | <b>Type C Interior</b> |      | <b>Type C Exterior</b> |  |
|                                | $\pm 1\sigma$ |      | $\pm 1\sigma$ |      | $\pm 1\sigma$          |      | $\pm 1\sigma$          |  |
| <i>n</i>                       | 18            |      | 10            |      | 5                      |      | na*                    |  |
| SiO <sub>2</sub>               | 41.27         | 0.74 | 41.88         | 2.20 | 40.21                  | 0.43 |                        |  |
| TiO <sub>2</sub>               | 2.01          | 0.18 | 1.87          | 0.20 | 2.06                   | 0.14 |                        |  |
| Al <sub>2</sub> O <sub>3</sub> | 14.77         | 1.10 | 13.81         | 2.59 | 14.97                  | 0.40 |                        |  |
| Cr <sub>2</sub> O <sub>3</sub> | 0.01          | 0.01 | 0.01          | 0.01 | 0.00                   | 0.02 |                        |  |
| FeO                            | 10.00         | 0.96 | 10.79         | 2.04 | 9.75                   | 0.44 |                        |  |
| MnO                            | 0.12          | 0.03 | 0.18          | 0.14 | 0.11                   | 0.05 |                        |  |
| MgO                            | 15.21         | 0.43 | 14.65         | 0.72 | 15.23                  | 0.24 |                        |  |
| CaO                            | 11.96         | 0.21 | 11.66         | 0.42 | 11.96                  | 0.19 |                        |  |
| Na <sub>2</sub> O              | 2.44          | 0.07 | 2.30          | 0.34 | 2.45                   | 0.07 |                        |  |

|                  |       |      |        |      |       |      |
|------------------|-------|------|--------|------|-------|------|
| K <sub>2</sub> O | 0.25  | 0.02 | 0.23   | 0.05 | 0.24  | 0.03 |
| Cl               | 0.06  | 0.01 | 0.07   | 0.03 | 0.08  | 0.05 |
| F                | 0.01  | 0.01 | 0.03   | 0.04 | n.a.  |      |
| Total            | 98.09 |      | 100.25 |      | 99.88 |      |

**c) Clinopyroxene**

|                                | Type A        |               | Type B        |               | Type C Interior |               | Type C Exterior |               |
|--------------------------------|---------------|---------------|---------------|---------------|-----------------|---------------|-----------------|---------------|
|                                | $\pm 1\sigma$ | $\pm 1\sigma$ | $\pm 1\sigma$ | $\pm 1\sigma$ | $\pm 1\sigma$   | $\pm 1\sigma$ | $\pm 1\sigma$   | $\pm 1\sigma$ |
| <i>n</i>                       | 9             |               | 9             |               | 5               |               | 8               |               |
| SiO <sub>2</sub>               | 49.21         | 1.48          | 50.37         | 1.86          | 47.38           | 1.40          | 47.96           | 2.01          |
| TiO <sub>2</sub>               | 0.80          | 0.28          | 0.64          | 0.26          | 0.95            | 0.35          | 0.90            | 0.39          |
| Al <sub>2</sub> O <sub>3</sub> | 4.73          | 1.72          | 4.16          | 2.62          | 6.07            | 2.14          | 5.42            | 2.35          |
| FeO                            | 10.09         | 2.39          | 10.04         | 1.44          | 9.25            | 1.60          | 9.58            | 1.17          |
| MnO                            | 0.37          | 0.20          | 0.41          | 0.19          | 0.29            | 0.20          | 0.31            | 0.10          |
| MgO                            | 14.50         | 1.17          | 14.39         | 0.88          | 14.06           | 0.69          | 14.41           | 1.37          |
| CaO                            | 19.76         | 2.19          | 19.80         | 1.36          | 20.46           | 1.46          | 19.91           | 1.60          |
| Na <sub>2</sub> O              | 0.27          | 0.05          | 0.31          | 0.17          | 0.25            | 0.01          | 0.24            | 0.04          |
| Total                          | 99.75         |               | 100.87        |               | 98.76           |               | 98.82           |               |

**d) Oxides**

|                                | Type A        |               | Type B        |               | Type C Interior |               | Type C Exterior |               |
|--------------------------------|---------------|---------------|---------------|---------------|-----------------|---------------|-----------------|---------------|
|                                | $\pm 1\sigma$ | $\pm 1\sigma$ | $\pm 1\sigma$ | $\pm 1\sigma$ | $\pm 1\sigma$   | $\pm 1\sigma$ | $\pm 1\sigma$   | $\pm 1\sigma$ |
| <i>n</i>                       | 10            |               | 17            |               | na              |               | 6               |               |
| SiO <sub>2</sub>               | 0.10          | 0.02          | 0.44          | 1.12          |                 |               | 0.32            | 0.62          |
| TiO <sub>2</sub>               | 9.33          | 2.53          | 9.26          | 2.92          |                 |               | 9.40            | 1.83          |
| Al <sub>2</sub> O <sub>3</sub> | 4.15          | 1.02          | 2.16          | 0.25          |                 |               | 2.31            | 0.33          |
| FeO                            | 79.69         | 1.66          | 81.75         | 3.52          |                 |               | 81.18           | 2.37          |
| MnO                            | 1.65          | 0.26          | 1.24          | 0.36          |                 |               | 1.57            | 0.13          |
| MgO                            | 0.39          | 0.04          | 0.52          | 0.09          |                 |               | 0.54            | 0.05          |

|       |       |      |       |      |  |       |      |
|-------|-------|------|-------|------|--|-------|------|
| CaO   | 0.05  | 0.04 | 0.07  | 0.07 |  | 0.07  | 0.06 |
| Total | 95.38 |      | 95.46 |      |  | 95.41 |      |

**e) Glass**

|                                | Type A        |      | Type B        |      | Type C<br>Interior |      | Type C<br>Exterior |      |
|--------------------------------|---------------|------|---------------|------|--------------------|------|--------------------|------|
|                                | $\pm 1\sigma$ |      | $\pm 1\sigma$ |      | $\pm 1\sigma$      |      | $\pm 1\sigma$      |      |
| <i>n</i>                       | 26            |      | 14            |      | 7                  |      | 7                  |      |
| SiO <sub>2</sub>               | 75.05         | 1.38 | 77.05         | 1.29 | 74.46              | 0.40 | 75.52              | 0.90 |
| TiO <sub>2</sub>               | 0.63          | 0.14 | 0.39          | 0.05 | 0.64               | 0.10 | 0.51               | 0.05 |
| Al <sub>2</sub> O <sub>3</sub> | 12.21         | 0.65 | 11.50         | 0.43 | 12.07              | 0.27 | 11.75              | 0.28 |
| FeO                            | 2.20          | 0.30 | 1.63          | 0.23 | 2.42               | 0.11 | 2.26               | 0.28 |
| MgO                            | 0.23          | 0.18 | 0.11          | 0.04 | 0.31               | 0.05 | 0.15               | 0.12 |
| MnO                            | 0.05          | 0.06 | 0.06          | 0.04 | 0.06               | 0.04 | 0.12               | 0.07 |
| CaO                            | 1.18          | 0.41 | 1.01          | 0.32 | 1.42               | 0.12 | 1.52               | 0.14 |
| Na <sub>2</sub> O              | 4.16          | 0.47 | 3.61          | 0.16 | 4.00               | 0.17 | 3.91               | 0.11 |
| K <sub>2</sub> O               | 3.83          | 0.55 | 2.98          | 0.10 | 2.89               | 0.08 | 2.68               | 0.16 |
| P <sub>2</sub> O <sub>5</sub>  | 0.13          | 0.11 | 0.11          | 0.25 | 0.22               | 0.08 | 0.22               | 0.09 |
| Cl                             | 0.35          | 0.17 | 0.46          | 0.11 | 0.52               | 0.08 | 0.47               | 0.08 |
| Total                          | 100.13        |      | 99.04         |      | 99.15              |      | 99.23              |      |

\*na: not available

**Table 6. Selected Phase IV and V XRF analyses**

| Sample no:                     | MVO1535d | MVO1535e | MT27     | MT29     | MVO1567d | MT35     | MVO1566b | MT37b    | MT09a    | MT25b    | MVO1593  |
|--------------------------------|----------|----------|----------|----------|----------|----------|----------|----------|----------|----------|----------|
| Eruption date                  | Jan-2009 | Jan-2009 | Feb-2010 | Feb-2010 | Feb-2010 | Feb-2010 | Dec-2009 | Feb-2010 | Feb-2010 | Feb-2010 | Feb-2010 |
| Type                           |          |          | A        | A        | A        | A        | A        | A        | B        | B        | B        |
| wt%                            |          |          |          |          |          |          |          |          |          |          |          |
| SiO <sub>2</sub>               | 53.85    | 53.47    | 49.54    | 51.60    | 51.50    | 52.01    | 51.96    | 52.84    | 56.24    | 57.22    | 54.72    |
| TiO <sub>2</sub>               | 0.97     | 0.77     | 0.88     | 0.80     | 0.82     | 0.80     | 0.79     | 0.80     | 0.67     | 0.66     | 0.73     |
| Al <sub>2</sub> O <sub>3</sub> | 16.17    | 19.17    | 20.09    | 19.12    | 19.67    | 19.63    | 19.68    | 19.59    | 18.74    | 18.52    | 18.79    |
| Fe <sub>2</sub> O <sub>3</sub> | 11.31    | 8.61     | 9.09     | 10.37    | 8.93     | 8.55     | 8.29     | 8.64     | 7.60     | 7.53     | 8.26     |
| MnO                            | 0.24     | 0.17     | 0.16     | 0.23     | 0.17     | 0.16     | 0.21     | 0.17     | 0.16     | 0.17     | 0.18     |
| MgO                            | 4.44     | 4.54     | 5.63     | 4.15     | 5.05     | 4.83     | 4.35     | 4.76     | 3.61     | 3.35     | 4.05     |
| CaO                            | 8.21     | 9.6      | 11.12    | 9.58     | 10.33    | 10.11    | 10.18    | 9.92     | 8.54     | 8.15     | 8.98     |
| Na <sub>2</sub> O              | 3.29     | 3.11     | 2.71     | 3.18     | 2.78     | 2.93     | 3.16     | 2.74     | 3.24     | 3.49     | 3.24     |
| K <sub>2</sub> O               | 0.6      | 0.54     | 0.41     | 0.42     | 0.54     | 0.55     | 0.45     | 0.62     | 0.67     | 0.74     | 0.61     |
| P <sub>2</sub> O               | 0.24     | 0.11     | 0.09     | 0.18     | 0.11     | 0.10     | 0.08     | 0.11     | 0.12     | 0.13     | 0.12     |
| LOI                            | †na      | na       | -0.11    | -0.33    | -0.28    | -0.29    | 0.10     | 1.06     | 0.01     | -0.36    | 0.08     |
| Total                          | 100.09   | 100.26   | 99.61    | 99.30    | 99.62    | 99.38    | 99.25    | 101.25   | 99.60    | 99.60    | 99.68    |
| ppm                            |          |          |          |          |          |          |          |          |          |          |          |
| Sc                             | 25       | 22       | 35       | 19       | 29       | 27       | 24       | 25       | 19       | 15       | 21       |
| V                              | 214      | 206      | 283      | 171      | 242      | 239      | 221      | 221      | 167      | 153      | 193      |
| Cu                             | bd       | 35       | 53       | 70       | 105      | 36       | 81       | 11       | bd       | bd       | 11       |
| Zn                             | 92       | 61       | 60       | 80       | 61       | 64       | 62       | 61       | 63       | 60       | 64       |
| Rb                             | 12       | 10       | *bd      | 10       | 13       | 10       | bd       | 15       | 14       | 16       | 12       |
| Sr                             | 233      | 267      | 273      | 299      | 270      | 272      | 274      | 264      | 261      | 262      | 268      |
| Y                              | 41       | 19       | 19       | 24       | 20       | 19       | 24       | 20       | 19       | 19       | 19       |
| Zr                             | 146      | 69       | 54       | 62       | 66       | 61       | 53       | 69       | 89       | 88       | 77       |
| Ba                             | 117      | 101      | 34       | 38       | 55       | 72       | 84       | 82       | 142      | 145      | 111      |
| Ce                             | 58       | 43       | 32       | 40       | 36       | 34       | 42       | 41       | 47       | 51       | 44       |

\*bd: below detection; †na: not available

| <b>MVO1566e</b> | <b>MT37a</b> | <b>MT11</b> | <b>MT08a</b> | <b>MT08b</b> |
|-----------------|--------------|-------------|--------------|--------------|
| Feb-2010        | Feb-2010     | Feb-2010    | Feb-2010     | Feb-2010     |
| B               | B            | B           | C            | C            |
| 54.14           | 56.61        | 55.30       | 52.88        | 55.58        |
| 0.74            | 0.66         | 0.74        | 0.78         | 0.73         |
| 19.20           | 18.77        | 18.43       | 19.30        | 18.55        |
| 8.10            | 7.64         | 8.21        | 8.38         | 8.22         |
| 0.16            | 0.17         | 0.18        | 0.17         | 0.18         |
| 4.11            | 3.57         | 4.02        | 4.57         | 4.01         |
| 9.27            | 8.44         | 8.73        | 9.74         | 8.74         |
| 3.13            | 3.39         | 3.10        | 3.02         | 3.23         |
| 0.60            | 0.78         | 0.65        | 0.54         | 0.64         |
| 0.11            | 0.13         | 0.12        | 0.11         | 0.13         |
| 0.12            | -0.25        | 0.04        | -0.06        | -0.01        |
| 99.56           | 100.00       | 99.52       | 99.66        | 99.43        |
| 21              | 17           | 23          | 27           | 20           |
| 207             | 163          | 207         | 232          | 185          |
| 25              | bd           | bd          | bd           | bd           |
| 62              | 63           | 69          | 66           | 66           |
| 11              | 19           | 14          | 11           | 13           |
| 270             | 262          | 256         | 266          | 261          |
| 18              | 18           | 20          | 21           | 21           |
| 72              | 82           | 82          | 70           | 81           |
| 106             | 135          | 128         | 82           | 119          |
| 35              | 43           | 47          | 46           | 45           |